De novo missense variants in exon 9 of *SEPHS1* cause a neurodevelopmental condition with developmental delay, poor growth, hypotonia, and dysmorphic features

Authors

Sureni V. Mullegama, Kaitlyn A. Kiernan, Erin Torti, ..., Kristin G. Monaghan, Jun Yang, Jane Juusola

Correspondence

smullegama@genedx.com (S.V.M.), junyang@utmb.edu (J.Y.)

***SEPHS1* is in the selenocysteine biosynthetic pathway. We report nine individuals from eight families with developmental delay, growth and feeding problems, hypotonia, and dysmorphic features, all with heterozygous missense variants in *SEPHS1*. Our findings provide insight into the molecular pathogenesis of this neurodevelopmental disorder.**

Mullegama et al., 2024, The American Journal of Human Genetics *111*, 778–790
April 4, 2024

https://doi.org/10.1016/j.ajhg.2024.02.016

CellPress

De novo missense variants in exon 9 of *SEPHS1* cause a neurodevelopmental condition with developmental delay, poor growth, hypotonia, and dysmorphic features

Sureni V. Mullegama,[1,2,23,*] Kaitlyn A. Kiernan,[3,23] Erin Torti,[1] Ethan Pavlovsky,[2] Nicholas Tilton,[2] Austin Sekula,[2] Hua Gao,[1] Joseph T. Alaimo,[4,5,6] Kendra Engleman,[5,7] Eric T. Rush,[5,7,8] Karli Blocker,[9] Katrina M. Dipple,[10] Veronica M. Fettig,[11] Heather Hare,[12] Ian Glass,[10] Dorothy K. Grange,[13] Michael Griffin,[2] Chanika Phornphutkul,[14] Lauren Massingham,[14] Lakshmi Mehta,[15,21] Danny E. Miller,[10] Jenny Thies,[16] J Lawrence Merritt II,[10] Eric Muller II,[9] Matthew Osmond,[17] Sarah L. Sawyer,[18] Rachel Slaugh,[13] Rachel E. Hickey,[19] Barry Wolf,[19] Care4Rare Canada Consortium, Undiagnosed Diseases Network, Sanjeev Choudhary,[2] Miljan Simonović,[3,22] Yueqing Zhang,[20] Timothy Blake Palculict,[1] Aida Telegrafi,[1] Deanna Alexis Carere,[1] Ingrid M. Wentzensen,[1] Michelle M. Morrow,[1] Kristin G. Monaghan,[1] Jun Yang,[20,*] and Jane Juusola[1]

Summary

Selenophosphate synthetase (SEPHS) plays an essential role in selenium metabolism. Two mammalian SEPHS paralogues, SEPHS1 and SEPHS2, share high sequence identity and structural homology with SEPHS. Here, we report nine individuals from eight families with developmental delay, growth and feeding problems, hypotonia, and dysmorphic features, all with heterozygous missense variants in SEPHS1. Eight of these individuals had a recurrent variant at amino acid position 371 of SEPHS1 (p.Arg371Trp, p.Arg371Gln, and p.Arg371Gly); seven of these variants were known to be *de novo*. Structural modeling and biochemical assays were used to understand the effect of these variants on SEPHS1 function. We found that a variant at residue Trp352 results in local structural changes of the C-terminal region of SEPHS1 that decrease the overall thermal stability of the enzyme. In contrast, variants of a solvent-exposed residue Arg371 do not impact enzyme stability and folding but could modulate direct protein-protein interactions of SEPSH1 with cellular factors in promoting cell proliferation and development. In neuronal SH-SY5Y cells, we assessed the impact of SEPHS1 variants on cell proliferation and ROS production and investigated the mRNA expression levels of genes encoding stress-related selenoproteins. Our findings provided evidence that the identified SEPHS1 variants enhance cell proliferation by modulating ROS homeostasis. Our study supports the hypothesis that SEPHS1 plays a critical role during human development and provides a basis for further investigation into the molecular mechanisms employed by SEPHS1. Furthermore, our data suggest that variants in SEPHS1 are associated with a neurodevelopmental disorder.

Selenium (Se) is the sole essential trace element to be specified in the genetic code[1] and is incorporated into proteins as the nonstandard amino acid selenocysteine (Sec) which is encoded by the UGA codon.[2–9] The human genome encodes 25 selenoproteins, many of which are involved in metabolism, maintenance of the cellular redox environment, and oxidative stress management.[10–13] The Sec biosynthesis machinery is responsible for generating Sec-tRNA^{Sec} and delivering it to the ribosome for incorporation into the nascent polypeptide chain.[2–4] The primary Se donor for Sec biosynthesis is provided by selenophosphate synthetase (SEPHS). Using ATP and inorganic Se as substrates, SEPHS cleaves and transfers the γ-phosphate of ATP onto selenide to form mono-selenophosphate (SeP).

[1]GeneDx, Gaithersburg, MD 20877, USA; [2]Department of Molecular and Cellular Biology, College of Osteopathic Medicine, Sam Houston State University, Conroe, TX 77304, USA; [3]Department of Biochemistry and Molecular Genetics, University of Illinois at Chicago, Chicago, IL 60607, USA; [4]Department of Pathology and Laboratory Medicine, Children's Mercy Hospital, Kansas City, MO, USA; [5]Department of Pediatrics, University of Missouri Kansas City, School of Medicine, Kansas City, MO, USA; [6]Center for Pediatric Genomic Medicine, Children's Mercy Hospital, Kansas City, MO, USA; [7]Division of Clinical Genetics, Children's Mercy Hospital, Kansas City, MO, USA; [8]Department of Internal Medicine, University of Kansas School of Medicine, Kansas City, KS, USA; [9]Division of Clinical Genetics, Stanford Children's Health, San Francisco, CA, USA; [10]Department of Pediatrics, Division of Genetic Medicine, University of Washington and Seattle Children's Hospital, Seattle, WA, USA; [11]Center for Inherited Cardiovascular Disease, Cardiovascular Genetics Program, Icahn School of Medicine at Mount Sinai, New York, NY, USA; [12]Northeastern Ontario Medical Genetics Program, Health Sciences, North Sudbury, ON, Canada; [13]Division of Genetics and Genomic Medicine, Department of Pediatrics, Washington University School of Medicine, St. Louis, MO, USA; [14]Division of Genetics, Department of Pediatrics, Alpert School of Medicine at Brown University, Providence, RI, USA; [15]Department of Genetics and Genomic Sciences, Icahn School of Medicine at Mount Sinai, New York, NY, USA; [16]Division of Genetic Medicine, Seattle Children's Hospital, Seattle, WA, USA; [17]Children's Hospital of Eastern Ontario Research Institute, University of Ottawa, Ottawa, ON, Canada; [18]Department of Pediatrics, University of Ottawa, Ottawa, ON, Canada; [19]Department of Pediatrics, Division of Genetics, Birth Defects and Metabolism, Anne & Robert H. Lurie Children's Hospital, Chicago, IL, USA; [20]Department of Internal Medicine, University of Texas Medical Branch, Galveston, TX 77555, USA
[21]Present address: Division of Clinical Genetics, Department of Pediatrics, Morgan Stanley Children's Hospital and Columbia University Medical Center, New York, New York, USA
[22]Present address: National Institutes of Health, National Institute of General Medical Sciences, Bethesda, MD 20892, USA
[23]These authors contributed equally
*Correspondence: smullegama@genedx.com (S.V.M.), junyang@utmb.edu (J.Y.)
https://doi.org/10.1016/j.ajhg.2024.02.016.

SeP is then delivered to *O*-phosphoseryl selenium transferase (SEPSECS) for the terminal reaction of Sec synthesis and subsequent incorporation into selenoproteins.[7]

Impairment in the Sec pathway has been associated with diverse human diseases including cardiovascular, central nervous, and endocrine system disorders, cancer, and pregnancy complications (miscarriage, premature birth, and preeclampsia).[1,6–13] Currently, three genes in the Sec biosynthesis pathway have been identified to cause autosomal-recessive disease: *SECISBP2* (MIM: 607693), *SEPSECS* (MIM: 613009), and *TRU-TCA1-1* (MIM: 620198).[10,12,14–17] Defects in *SECISBP2* are associated with an abnormal thyroid hormone metabolism disorder (MIM: 609698),which is characterized by multiorgan defects including abnormal thyroid hormone metabolism, myopathy, hearing loss, and male infertility.[15] *SEPSECS* pathogenic variants are associated with pontocerebellar hypoplasia type 2D (MIM: 613811) which is characterized by progressive microcephaly, postnatal onset of progressive atrophy of the cerebrum and cerebellum, profound intellectual delay, spasticity, and variable seizures.[14,18] Pathogenic variants in *TRU-TCA1-1* are associated with autosomal-recessive thyroid hormone metabolism, abnormal 3 (MIM: 165060) which is characterized by euthyroid hyperthyroxinemia, with elevated free T4 and reverse T3 levels and normal TSH (MIM: 188540) and free T3 levels.[16,17] Affected individuals also show low plasma selenium levels and reduced levels of stress-related selenoproteins[16,17]

In the human Sec biosynthesis pathway, there are two *SEPHS* genes encoding *SEPHS1* and *SEPHS2* that both share a high degree of sequence identity and structural homology. However, it has been established that SEPHS2 catalyzes SeP synthesis.[19,20] Due to the implications of the Sec biosynthesis pathway to human disease, variants in *SEPHS1* (MIM: 600902) or *SEPHS2* (MIM: 606218) may be linked to a genetic disorder. Interestingly, these two genes have yet to be implicated in human disease in OMIM.

SEPHS1 is an essential protein in mammals and is involved in promoting cell proliferation, differentiation, and survival.[21–24] SEPHS1 has been found to modulate the cellular redox environment and promote cell migration, adhesion, and invasion.[21,24] It is highly expressed in hepatocytes and thyroid glandular cells. The gene is ubiquitously expressed in the brain but has no region specificity.[21,25] In *Drosophila melanogaster, Sps1* is highly expressed during embryonic development and is prevalent in regions of the embryo undergoing rapid cell proliferation and differentiation.[26]

Given the fact that SEPHS1 does not directly participate in generating SeP, it is reasonable to propose that SEPHS1 plays a critical role in cellular processes outside of the Sec biosynthetic pathway. It has been found SEPHS1 modulates redox homeostasis and is responsible for cell proliferation and defense.[19,20,25] However, the homeostatic mechanism by which this protein exerts its function is still poorly understood.

Sephs1 knockout mice embryos showed gradual increases in reactive oxygen species (ROS) resulting in growth retardation, structural brain abnormalities, and disrupted cardiac development.[23,27] Therefore, it is likely that in humans, *SEPHS1* is an essential gene and pathogenic variants may cause a human phenotype resembling other disorders in the Sec biosynthesis pathway.

In this study, nine individuals were identified to have heterozygous missense variants in *SEPHS1* by clinical exome sequencing (ES) (see supplemental material and methods). They were evaluated by clinical genetic centers in the United States and Canada via clinical exam, laboratory tests, and brain imaging. Clinical data were obtained from the providers via questionnaire. This study was approved by the institutional review board (IRB) (see supplemental material and methods). All parents or legal guardians provided written informed consent for their children to participate in the study and for publication of clinical information. Seven individuals (individuals 1–4 and 7–9) had ES performed by GeneDx. Individual 5 had ES performed at a pediatric medical center and was ascertained via personal communication. Individual 6 had ES performed through Care4Rare and was ascertained via GeneMatcher.[28]

Eight individuals (individuals 1–8) had variants at the same amino acid position, p.Arg371 (Table 1). Individuals 1–3 shared a recurrent variant in *SEPHS1* (GenBank: NM_012247.4: c.1111C>T [p.Arg371Trp]). This variant was *de novo* in individuals 1 and 2, but parental testing for individual 3 was not available (Figures S1A and S1B). Individuals 4–6 shared a different missense variant at the same residue in *SEPHS1* (GenBank: NM_012247.4: c.1112G>A [p.Arg371Gln]). This variant was *de novo* in individuals 4–6 (Figures S1D and S1E). Individuals 7 and 8 were similarly affected siblings who shared a third unique missense variant at the p.Arg371 residue in *SEPHS1* (GenBank: NM_012247.4: c.1111C>G [p.Arg371Gly]) (Figures S1F and S1G). This variant was *de novo* in the siblings, suggesting the possibility of parental germline mosaicism in this family. In addition, individual 7 had a *de novo* *SRCAP* (MIM: 611421) variant, GenBank: NM_006662.2 (c.3833C>A [p.Ser1278*]), that was classified as a variant of uncertain significance (VUS).[29] Individual 9 had a *de novo* missense variant at a different residue in *SEPHS1* (GenBank: NM_012247.4: c.1054T>G [p.Trp352Gly]) (Figure S1H). All variants were located within exon 9 of *SEPHS1* and located in/near the region encoding the AIR synthase-related protein, C-terminal domain of SEPHS1 (Figure 1A). None of these variants were reported in Genome Aggregation Database v.4.0.0 (gnomAD). *SEPHS1* contains fewer missense variants than expected (Z score = 3.24) and is considered intolerant to loss of function (pLI = 0.98).[30] The gene has a relatively %HI score implying that it is likely that variants within this gene operate through a mechanism of haploinsufficiency.[31] The *in silico* prediction tool Provean predicts each of the identified missense changes to have a deleterious effect on *SEPHS1* (Table 1).

Table 1. Molecular findings in individuals with heterozygous missense *SEPHS1* variants

	Individual 1	Individual 2	Individual 3	Individual 4	Individual 5	Individual 6	Individual 7	Individual 8	Individual 9
SEPHS1 variant (NM_012247.4)	c.1111C>T	c.1111C>T	c.1111C>T	c.1112G>A	c.1112G>A	c.1112G>A	c.1111C>G	c.1111C>G	c.1054T>G
Exon	exon 9	exon 9	exon 9	exon 9	exon 9	exon 9	exon 9	exon 9	exon 9
Protein	p.Arg371Trp	p.Arg371Trp	p.Arg371Trp	p.Arg371Gln	p.Arg371Gln	p.Arg371Gln	p.Arg371Gly	p.Arg371Gly	p.Trp352Gly
Inheritance	*de novo*	*de novo*	unknown	*de novo*	*de novo*	*de novo*	*de novo*	*de novo*	*de novo*
PROVEAN (cutoff 2.5)	−3.75	−3.75	−3.75	−1.15	−1.15	−1.15	−3.65	−3.65	−10.49
GnomAD frequency	0	0	0	0	0	0	0	0	0
Reported CNV and SNVs	none reported	none reported	CMA: gain of chr13q14.1 (VUS, unknown inheritance)[a]	none reported	none reported	CMA: gain of chr3p25.3 (VUS, maternally inherited)[a]	*de novo* VUS in *SRCAP*, NM_006662.2: c.3833C>A (p.Ser1278*)[29]	none reported	heteroplasmic variant in *MT-TL2*; heterozygous VUS *RAPSN*[a]
ACMG criteria applied[33]	internal criteria, PM2, PP3	internal criteria, PM2, PP3	internal criteria, PM2, PP3	internal criteria, PS2, PM2, BP4	internal criteria, PS2, PM2, BP4	internal criteria, PS2, PM2, BP4	internal criteria, PM2, PP3	internal criteria, PM2, PP3	PS2, PS3, PM2, PP3
ACMG Class	PATH	PATH	PATH	PATH	PATH	PATH	PATH	PATH	PATH
ClinVar accession	SCV002103293 .1	SCV002103293.1	SCV002103293.1	SCV002103295.1	SCV002103295.1	SCV002103295.1	SCV002103294.2	SCV002103294.2	SCV002103296.1

CMA, chromosomal microarray
[a]No HGVS notation available

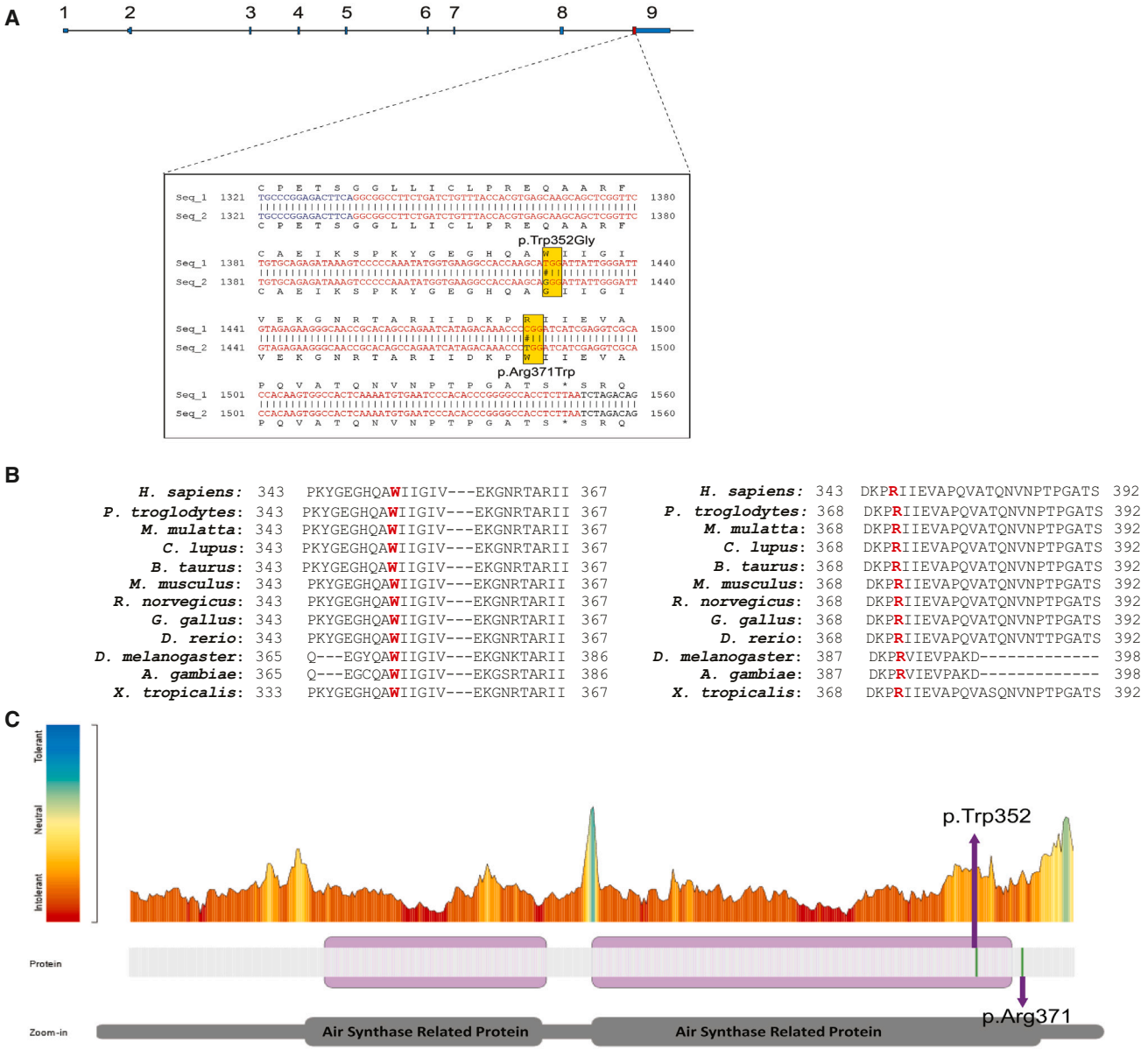

Figure 1. Identification of missense *SEPHS1* variants in nine individuals

(A) Schematic of *SEPHS1* organization. The blue boxes reflect exons. The yellow box depicts *SEPHS1* variant position.

(B) Evolutionary conservation of missense variants observed in SEPHS1. Protein alignment of SEPHS1 orthologs was performed to determine protein sequence conservation of the region of interests. Residues impacted by variants within our cohort are highlighted in red. The Trp352 and Arg371 amino acids are highly conserved from human to frog.

(C) Tolerance Landscape of SEPHS1. The tolerance landscape of SEPHS1 was generated using Metadome (https://stuart.radboudumc.nl/metadome/). The color in the plot is an indication for the tolerance (red, intolerant; blue, tolerant). Graphical representation of the linear protein structure of SEPHS1 with two functional Air Synthase Related Protein domains is below the plot. Missense variants observed in this study are labeled, p.Arg371 and p.Trp352G. The missense variants in SEPHS1 are located in regions that are intolerable for variation (red).

The amino acids at the two variant sites identified in the nine affected individuals (Trp352 and Arg371) are highly conserved throughout multiple species (Figure 1B) indicating that the tryptophan (Trp) and arginine (Arg) play an essential role in protein function. To identify the tolerance landscape of these missense variants, we utilized Metadome regional tolerance plot for genetic variation based on the ratio of observed missense and synonymous (*dN/dS*) variants that are included in gnomAD.[32] Both altered positions in *SEPHS1* are in regions that are intolerant to missense variants (Figure 1C).

The clinical features of the nine individuals are summarized in Tables 2 and S1 and Figure S2. The cohort is comprised of 5 females and 4 males. The ages of the cohort ranged from two days to 16 years. Individual 7 expired at two days of age due to complications of persistent pulmonary hypertension of the newborn (PPHN); therefore, most of the phenotypic comparison was made among the other

Table 2. Clinical characteristics of individuals with *SEPHS1* variants

Demographics	Individual 1	Individual 2	Individual 3	Individual 4	Individual 5	Individual6	Individual 7	Individual 8	Individual9
Age at last evaluation	2.5 years	23 months	8 years	11 years	16 years	7.6 years	2 days	3.5 years	4 years
Neurocognitive features									
Developmental delay	+	+	+	+	+	+	NR	+	+
Intellectual disability	NR	–	+	NR	+	possible[a]	NR	+	possible[a]
Neurobehavioral diagnoses	NR	NR	NR	NR	+	+	NR	NR	–
Hypotonia and/or muscle weakness	+	+	+	–	+	+	+	NR	+
Clinically significant brain malformation on MRI	NR	NR	–	–	–	NR	NR	–	–
Other neurologic findings	–	–	+	–	+	+	NR	NR	–
Growth-related features									
History of poor height growth	+	+	–	+	+	–	–	–	+
History of poor weight gain	+	+	–	+	+	–	NR	–	+
Feeding difficulties	+	+	+	–	+	+	NR	NR	+
Additional features									
Dysmorphic craniofacial features[b]	+	+	+	+	+	+	NR	NR	+
Endocrine	–	+	NR	+	+	NR	+	+	–
Respiratory	+	–	+	+	+	–	+	+	–
Ophthalmologic	+	–	–	NR	+	+	NR	NR	+
Cardiac	–	–	–	–	+	NR	+	+	–
Gastrointestinal	+	–	+	+	–	–	NR	NR	NR

NR, data not reported
[a]No formal assessment of intellectual disability
[b]Dysmorphic facial features are described in Table S1

individuals. Despite the small sample size, there was a remarkably strong clinical overlap (Table 2; Figure S2). The most consistent feature observed in our cohort was developmental delay (8/8; 100%), with five of those individuals known or suspected to have intellectual disability. Two of the affected individuals also had neurobehavioral diagnoses (attention-deficit/hyperactivity disorder in two; obsessive-compulsive disorder in one). Hypotonia and/or muscle weakness was reported in all but one affected individual. Additional neurologic/neuromuscular findings present in single affected individuals include petit mal seizures, lower limb myalgia and fatigue, autoimmune encephalitis, and decreased muscle mass. None of the affected individuals who underwent brain MRI (n = 5) had a major malformation. Growth was also widely impacted. Five affected individuals had a history of both poor height growth and weight gain, four of whom had history of feeding difficulties. Two individuals of typical size also had a history of feeding problems; tube feedings were required in three affected individuals. Multiple facial dysmorphisms were observed in seven affected individuals (Table S1). Issues affecting other body systems were more variable within the cohort. Endocrine abnormalities reported in a single affected individual include Hashimoto's thyroiditis (individual 5) and elevated B6 (individual 2). Two affected individuals had growth hormone deficiency (individuals 4 and 9) and the siblings had congenital hypocalcemia (individuals 7 and 8). Respiratory issues seen in multiple affected individuals include obstructive sleep apnea (n = 3), laryngomalacia (n = 2), recurrent pneumonia (n = 2), and asthma (n = 2). Gastrointestinal issues included constipation (n = 3) and anorectal malformation

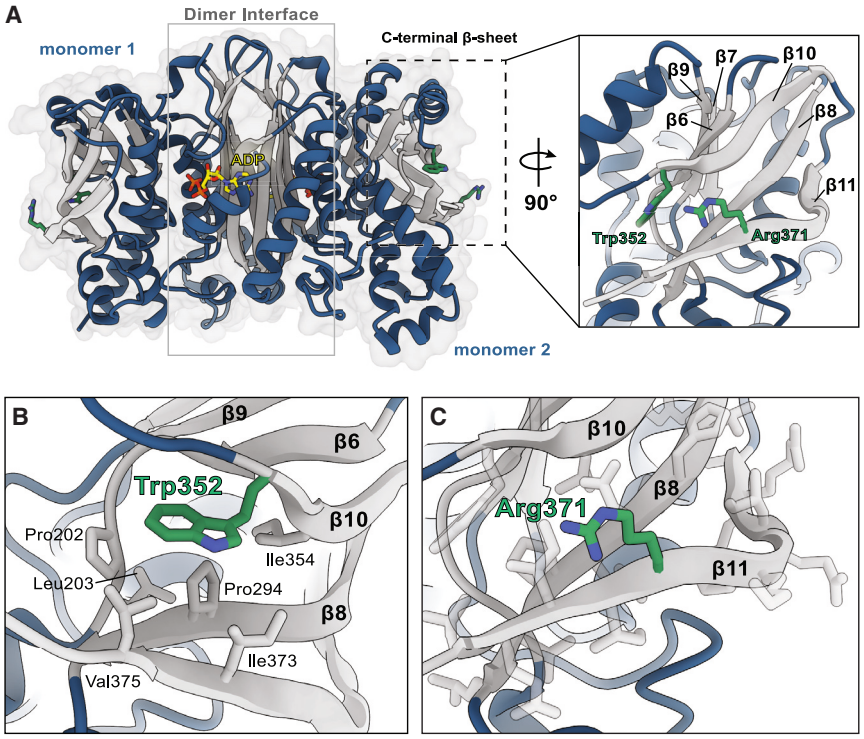

Figure 2. Structural modeling of SEPHS1

(A) Overall structural organization of SEPHS1 (PDB: 3FD6). Interactions between the N-terminal regions of monomers 1 and 2 form a β-barrel-like structure to stabilize the homodimer and active sites. ADP is shown in yellow. Residues Trp352 and Arg371 are situated in the C-terminal β-sheet and are highlighted in green.

(B) Trp352 resides in a hydrophobic pocket stabilized by interactions with neighboring hydrophobic residues.

(C) Arg371 is located on the solvent-exposed face of β11 and does not appear to form any significant interactions with surrounding residues. All modeling was performed using PyMOL (The PyMOL Molecular Graphics System, Version 2.0 Schrödinger, LLC).

(n = 1). Two affected individuals had myopia, and ophthalmologic issues reported in single affected individuals included strabismus, astigmatism, ptosis, and congenital entropion. Cardiac/vascular anomalies were seen in three affected individuals (aberrant right subclavian artery in one affected individual; persistent pulmonary hypertension of the newborn in the siblings), with three affected individuals having normal echocardiograms. Overall, it is likely that *de novo* variants in *SEPHS1* that disrupt SEPHS1 function result in a syndromic neurodevelopmental disorder. Suggestions for clinical care based on the medical and developmental histories of our cohort can be found in the supplemental note.

To further demonstrate whether these variants in *SEPHS1* disrupt SEPHS1 function, we investigated the effect of the variants on protein function by using both biochemical assays and structural modeling. When we mapped the location of the altered residues, we observed that both residues Trp352 and Arg371 are situated within a six-stranded β-sheet in the C-terminal domain (Figure 2A). The architecture of this β-sheet is notated as β7↑ β9↓ β6↑ β10↓ β8↑ β11↑ with Trp352 located on the N-terminal tail of β10 and Arg371 found in the middle of β11 (Figure 2A). The side chain of Trp352 makes extensive contacts with Pro202, Leu203, Pro294, Ile354, Ile373, and Val375, which contribute to the formation of a hydrophobic pocket that stabilizes three antiparallel β-strands β8, β10, and β11 (Figure 2B). By contrast, the side chain of Arg371 is solvent-exposed and does not appear to participate in any interactions stabilizing the enzyme structure (Figure 2C).

Given that affected residues are far removed from the dimer interface and active sites, we sought to determine how pathogenic *SEPSH1* variants may affect overall protein stability and architecture, local conformational stability, and enzyme function. Using site-directed mutagenesis, we recapitulated the *de novo* variants (p.Trp352Gly, p.Arg371Gly, p.Arg371Gln, and p.Arg371Trp) and wild-type (WT) SEPHS1 enzymes in *E. coli*. All proteins were purified with a combination of affinity and size-exclusion chromatography. The native PAGE analysis confirmed all variants maintained the native dimer form, with the expected molecular weight of ~85 kDa (Figure 3A). We then employed size-exclusion chromatography coupled with multi-angle light scattering (SEC-MALS) to accurately determine the molecular weight (MW) and polydispersity of all SEPHS1 samples. The average MW of all enzymes was calculated to be 85.41% ± 0.87% kDa with a polydispersity constant of 1.0% ± 0.001% (Figure S3), confirming that all recombinant SEPHS1 enzymes exist as dimers in solution.

Though not directly participating in the Sec biosynthetic pathway, SEPHS1 retains the ATPase activity. We investigated the possibility that pathogenic variants impact the active-site conformation and enzymatic activity. Using a luciferase-based ATPase assay, we monitored the relative change in ATP concentration over time. Our data show that WT, p.Trp352Gly, p.Arg371Gly, and p.Arg371Gln all consumed ~50%–60% of the available ATP over the course of the assay (Figure 3D). The p.Arg371Trp exhibited a moderate reduction in activity consuming only ~30% of the total ATP, suggestive of hypomorphic properties. Ultimately, we found all SEPHS1 variants are capable of hydrolyzing ATP *in vitro*, suggesting the dimer interface and active sites are not detrimentally impacted by the variants for this function.

To investigate whether the overall protein stability was altered by the variants, we used the Nanotemper

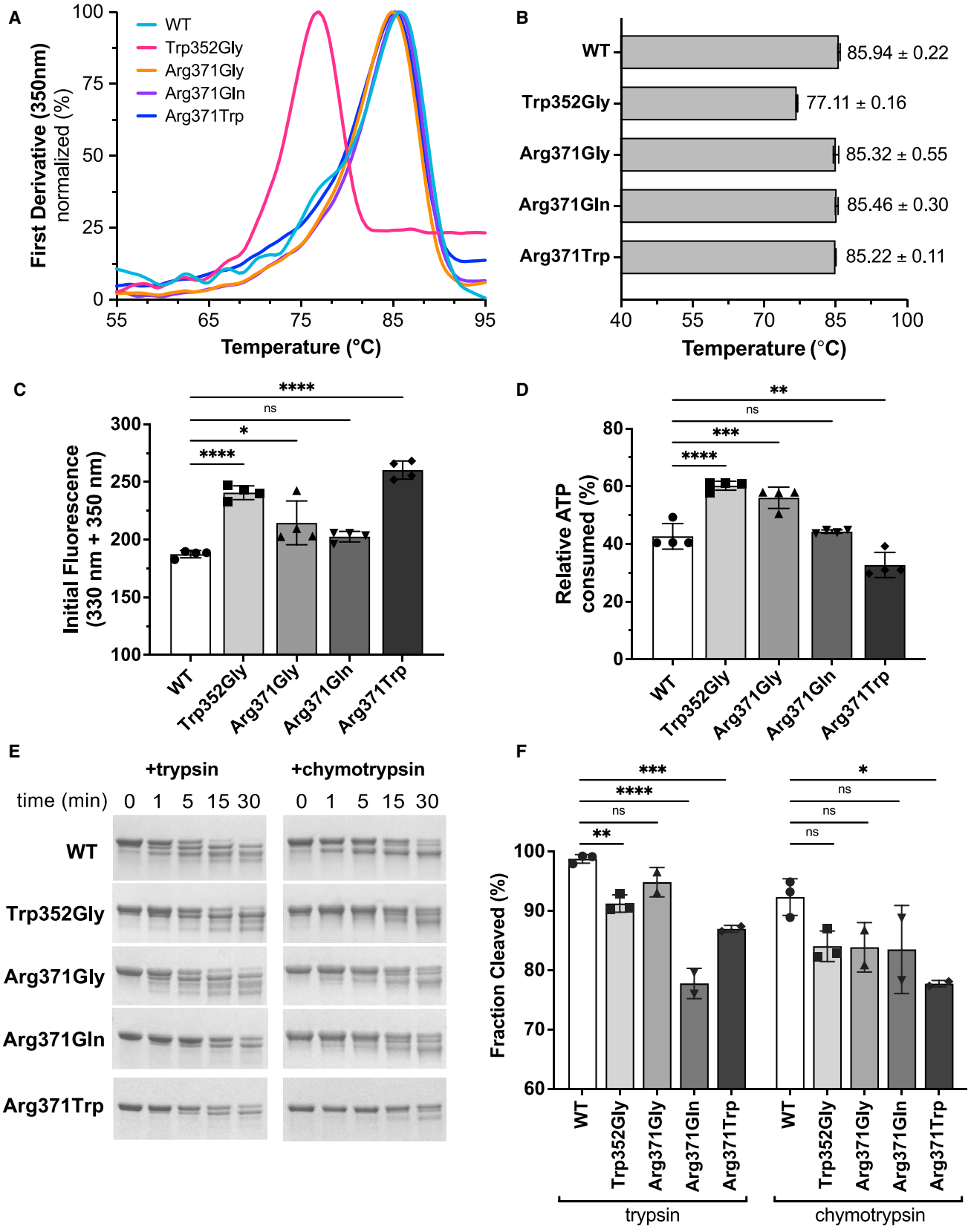

Figure 3. Analysis of SEPHS1 stability and enzymatic activity

(A) Protein thermal stability was measured using the Tycho NT.6 instrument. Intrinsic protein fluorescence was monitored as a thermal ramp was applied to each sample. The resulting curves are plotted as the first derivative and used to calculate the inflection temperature (Ti) for each sample.

(B) Calculated Ti values.

(legend continued on next page)

instrument Tycho NT.6 to monitor intrinsic fluorescence changes of each enzyme sample during heat denaturation. When comparing the inflection temperatures (Ti) of the variants to WT *SEPHS1*, we observed a substantial decrease (∼10°C) in p.Trp352Gly while there was very little change with any of the Arg371 variants (Figure 3B). As this method is based on the intrinsic fluorescence of Trp residues, we expected the initial fluorescence of the p.Trp352Gly variant would decrease as a Trp residue was removed. Unexpectedly, the initial fluorescence for p.Trp352Gly was significantly higher than WT SEPHS1 (Figure 3C). This suggests that the variant causes other Trp residues, which are normally buried in the WT protein, to be exposed in the altered enzyme. Furthermore, p.Arg371Gly exhibited a small increase in initial fluorescence, suggesting slight changes in the local environment surrounding residue 371 but not enough to reduce thermal stability of the entire protein.

These results led us to speculate that pathogenic variants may elicit local structural changes in the C-terminal region of SEPHS1. To probe this, we used limited proteolysis with trypsin and chymotrypsin proteases (Figure 3E). In comparison to WT, SEPHS1 variants exhibited similar cleavage patterns for both proteases but exhibited varying degrees of proteolytic resistance. p.Trp352Gly, p.Arg371Gln, and p.Arg371Trp variants exhibited the highest resistance to proteolytic cleavage. Taken together, our results suggest that Trp352 stabilizes the C-terminal domain of SEPSH1 and, when replaced with Gly, induces local structural changes across the 6-stranded β-sheet. While exhibiting small changes in initial fluorescence and resistance to proteolysis, most of the Arg371 variants did not have a significant impact on protein stability. Thus, we suggest Arg371 variant does not greatly compromise the structural integrity of the C-terminal β-sheet and instead may play an integral role in modulating protein-protein interactions in the cell.

To investigate the physiological functions of the *SEPHS1* variants, we introduced FLAG-tagged *SEPHS1* variants into human neuroblastoma SH-SY5Y cells through lentiviral-mediated transduction. We initiated our assessment by examining the impact of *SEPHS1* variants on cell proliferation using the alamarBlue viability assay (Figure 4A). The results indicated that the growth rate of p.Arg371Gln was comparable to that of the control and WT, while p.Trp352Gly, p.Arg371Gly, and p.Arg371Trp exhibited substantially increased cell proliferation, with p.Arg371Trp demonstrating the most pronounced effect among them. Furthermore, immunoprecipitation using the M2 anti-FLAG antibody revealed that the dimerization capability of FLAG-tagged SEPHS1 variants with endogenous SEPHS1 remained unaltered (Figure 4B). These findings align with our earlier observations from bacterial recombinant expression, indicating that the identified variants would not influence SEPHS1 functions by affecting SEPHS1 dimerization.

Given SEPHS1's pivotal role in regulating stress-related selenoproteins and maintaining redox homeostasis, we further investigated whether the identified variants influence cell proliferation through ROS production (Figure 4C). In the absence of oxidative stress stimulation, there were no significant differences in intracellular ROS production observed between the variants and WT (Figures 4C and 4D, top). Intriguingly, when the oxidant tBHP was employed in the cells to induce oxidative stress, p.Trp352Gly, p.Arg371Gly, and p.Arg371Trp exhibited a significant reduction in ROS production compared to WT. Among the variants, p.Arg371Trp displayed the most substantial reduction, while p.Arg371Gln had a marginal effect on tBHP-induced ROS production (Figures 4C and 4D, bottom).

The observed impact of *SEPHS1* variants on ROS accumulation prompted us to investigate the mRNA expression levels of genes encoding stress-related selenoproteins, specifically glutathione peroxidase 1 (*GPX1* [MIM: 138320]), glutathione peroxidase 4 (*GPX4* [MIM: 138322]), thioredoxin reductase 1 (*TXNRD1* [MIM: 601112]), selenoprotein T (*SELENOT* [MIM: 607912]), selenoprotein W (*SELENOW* [MIM: 603235]), and methionine sulfoxide reductase B1 (*MSRB1* [MIM: 606216]). Additionally, we examined the expression of genes encoding ROS-scavenging enzymes, including peroxiredoxin 1 (*PRDX1* [MIM: 176763]), glutathione S-transferase alpha 4 (*GSTA4* [MIM: 605450]), glutathione S-transferase omega 1 (*GSTO1* [MIM: 605482]), and superoxide dismutase 3 (*SOD3* [MIM: 185490]). Quantitative real-time PCR analysis revealed that the mRNA expression *of GPX1, MSRB1, SELENOW, SOD3, GPX4, MSBR1*, and *TXNRD1* was increased in the p.Trp352Gly, p.Arg371Gly, and p.Arg371Trp variants compared to the WT, whereas the expression of *GSTA4, GSTO1, PRDX1*, and *SELENOT* remained unaffected. Once again, the variant p.Arg371Gln exhibited little to no effect (Figure 4E).

In this study, we used ES to identify variants affecting the C-terminal region of SEPHS1 in nine individuals with an overlapping phenotype. The variants are classified as pathogenic based on the ACMG recommendations

(C) Initial fluorescence values measured for each sample using the Tycho NT.6. All Ti and initial fluorescence values are reported with ±SD from 4 independent runs.
(D) SEPHS1-mediated ATP hydrolysis monitored using the CellTiter-Glo Assay 2.0 assay kit. Relative ATP consumption was measured after 18 h of incubation at +37°C. Assays were performed in triplicates and reported with ±SD.
(E) Trypsin or chymotrypsin was added to SEPHS1 samples and allowed to digest the protein for 30 min. Time points were taken at 0, 1, 5, 15, and 30 min. Digested products were analyzed on 4%–20% TGX gels. Representative gels are shown from 2 to 3 independent cleavage reactions.
(F) Densitometric quantification performed with ImageJ of total fraction cleaved after 30 min. Statistical significance for all panels was determined by one-way ANOVA with the Bonferroni correction, *$p < 0.05$, **$p < 0.01$, ***$p < 0.001$, ****$p < 0.0001$.

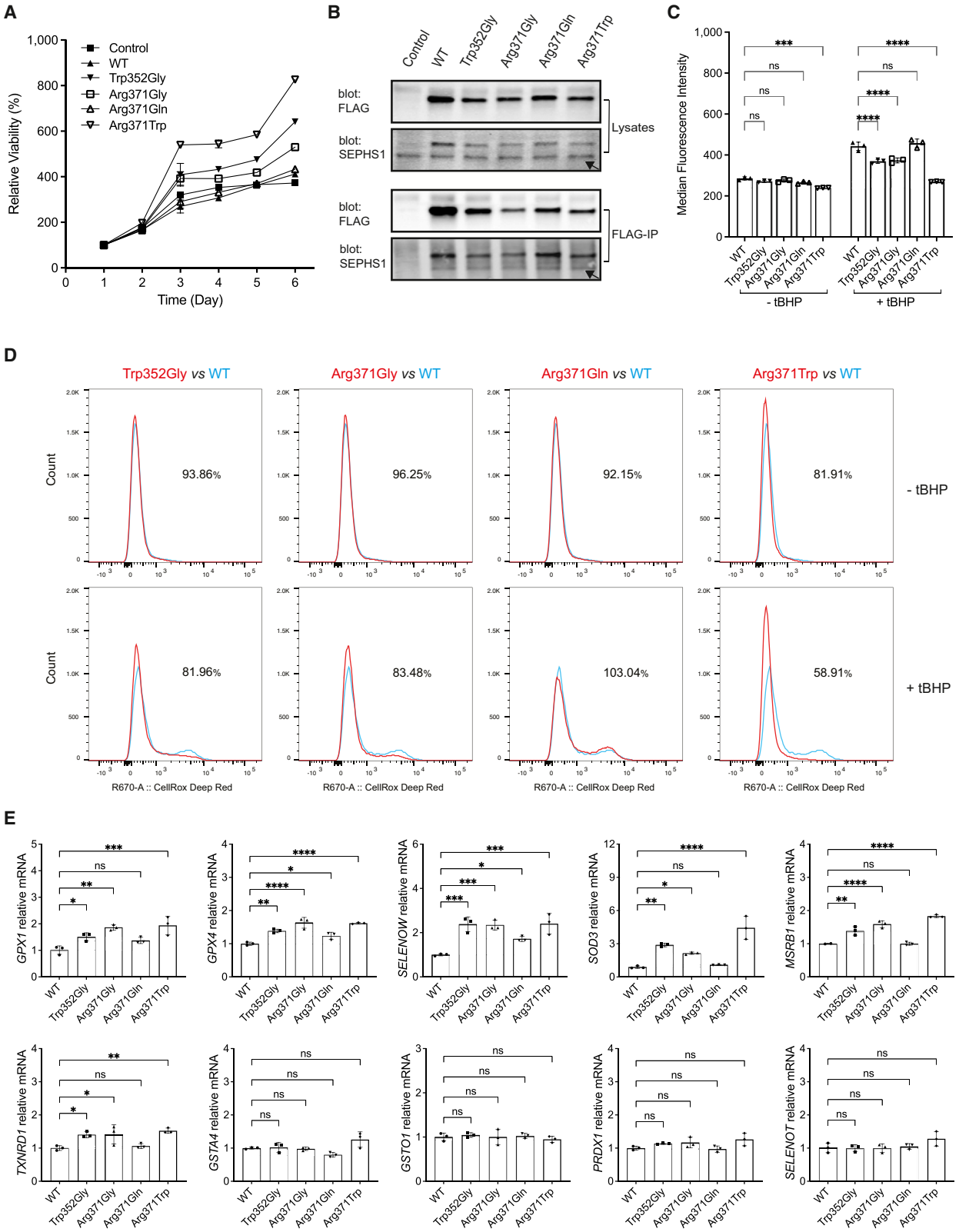

Figure 4. Analysis of SEPHS1 cellular functions in SH-SY5Y cells

(A) Cell proliferation analysis of SH-SY5Y cells overexpressing *SEPHS1* variants at the indicated days. The % live cell values were normalized to the day 1 cells (considered as 100% viable).

(B) Immunoblotting for immunoprecipitation of FLAG-tagged SEPHS1 variants. Arrows indicate the endogenous SEPHS1.

(C) Fluorescence-activated cell sorting (FACS) analysis of CellROX Deep Red fluorescence in SH-SY5Y cells with or without treatment with ROS inducer tBHP, showing the quantitative bar graphs and statistical analysis of the median fluorescence intensity (MFI). Error bars derived from three independent measurements.

(legend continued on next page)

for interpretating and reporting sequence variants (Table 1).[33]

Functional characterization revealed that variant p.Trp352Gly significantly reduced the overall thermal stability of the protein, due to the disruption of a network of hydrophobic interactions. When compared to WT SEPHS1, we determined that p.Trp352Gly was more resistant to proteolytic cleavage and found that the initial fluorescence of p.Trp352Gly was drastically enhanced due to the exposure of Trp residues that are usually buried in the core of the WT protein. Replacement of Trp352 with a Gly residue destabilizes a C-terminal hydrophobic pocket containing residues spanning the entire β-sheet, leading to local structural changes which may modulate protein-protein interactions in the cell. With eight out of nine individuals having Arg371 variants, it was intriguing to us that they behaved differently than p.Trp352Gly and resembled WT SEPHS1. Arg371 variants did not significantly affect protein stability or proteolytic cleavage pattern. Thus, we propose that Arg371 does not contribute to stabilization of the C-terminal region but rather likely participates in recognition and/or regulation of SEPHS1 binding partners. Our findings in neuronal SH-SY5Y cells provide evidence that the identified SEPHS1 variants could enhance cell proliferation by modulating ROS homeostasis. However, the specific impact of the p.Arg371Gln variant on cellular function remains unclear. Further investigation is needed to elucidate the precise mechanism by which SEPHS1 variants influence the expression of genes encoding stress-related selenoproteins and ROS-scavenging enzymes.

Based on the cellular data, the variants in SEPHS1 most likely act through a gain-of-function mechanism. Proper function of selenoproteins is shown to be crucial for neuronal function.[6,9,11,13,18,34] It is conceivable that defective *SEPHS1* could affect development of limbic system structure, including the hypothalamus, thalamus, basal ganglia, cingulate gyrus, hippocampus, and amygdala.[19,20] In addition, individuals with impaired function of *SEPHS1* may have neurodevelopmental deficits due to possible loss in the total number of pluripotent stem cells that survive during fetal development by an overactivation of the RAS/MAPK signaling pathway in these cells.[23] Additionally, a deficiency of growth hormone-releasing hormone and thyroid-stimulating hormone secondary to diminished hypothalamic input to the anterior pituitary gland may exacerbate the neurodevelopmental and growth delays seen in our cohort.[35–37]

SEPHS1 has high evolutionary conservation across species, which allows for the study of the gene in various animal models.[37] Based on findings from the *in vitro*, mouse, and fly models, SEPHS1 plays an essential role during cell development and proliferation and regulates cellular redox homeostasis and defense. *Sephs1*-targeted knockouts in the mice and the knockout of *Sps1* mRNA in *Drosophila* show neurodevelopment being affected as well as embryonic lethality.[23,26] Heterozygous *Sps1* variants in *Drosophila* resulted in eye phenotypes, which could coincide with the variable eye phenotypes seen in our cohort.

In mouse and human cells, knockdown of *SEPHS1* suppresses cell proliferation. *Sephs1* knockout mice had embryos that were underdeveloped by day E8.5 and virtually resorbed by day E14.5.[27] Knockdown of *Sephs1* mRNA in a *Drosophila* SL2 immortalized cell line led to the inhibition of cell proliferation.[26] In this model, megamitochondria were formed through the inhibition of pyridoxal phosphate which is the active form of vitamin B6 and necessary for SepSecS function, among other roles. Interestingly, one individual had elevated B6 levels. Taken together, our study helps support the role of SEPHS1 in human growth and development. In our study, individuals with *SEPHS1* pathogenic variants exhibit hypotonia, muscle weakness, poor weight gain, growth delays, and short stature. The phenotypes point to the role of SEPHS1 in regulating growth via modulation of ROS. In the Ras/MAPK signaling pathway, ROS are messengers for growth and gain-of-function variants in this pathway are associated with a group of disorders termed RASopathies.[38]

To gain a deeper understanding of the potential link between SEPHS1 variants and cell proliferation via alterations in ROS homeostasis, it is imperative to conduct future experiments either in cell culture systems or animal models. These experiments will provide a more comprehensive and certain insight into the underlying mechanisms at play. By examining specific ROS homeostasis mechanisms and the signaling pathways affected by *SEPHS1* variants, we can identify the precise molecular interactions responsible for the observed cellular changes. Additionally, a comparative analysis between cells with wild-type *SEPHS1* and those with *SEPHS1* variants will offer valuable insights into the differences in ROS regulation and cell proliferation rates, further confirming the role of these variants. Such investigations will not only advance our understanding of this neurodevelopmental disorder but also provide a foundation for the development of targeted therapeutic strategies aimed at restoring cellular homeostasis and improving patient outcomes.

Overall, individuals with pathogenic variants in *SEPHS1* appear to have a neurodevelopmental and growth disorder, with variable effects on other body systems. We provide some considerations for immediate and long-term care of these individuals (see supplemental note). In conclusion, missense variants in exon 9 of *SEPHS1*

(D) FACS histograms showing ROS production as described in (C). The numerical values accompanying each histogram signify the percentage of MFI for SEPHS1 variants relative to the wild-type (WT).
(E) Quantitative real-time PCR for genes encoding stress-related selenoproteins and ROS-scavenging enzymes in SH-SY5Y cells harboring *SEPHS1* variants. mRNA levels were normalized to *PolB*. Data are represented as mean ± SEM, n = 3. *$p < 0.05$, **$p < 0.01$, ***$p < 0.001$, ****$p < 0.0001$ and ns, not statistically significant.

underlie a neurodevelopmental syndrome associated with developmental delay, growth problems, feeding difficulties, hypotonia, and dysmorphic features. Our findings provide insight into the molecular pathogenesis of this disorder.

Data and code availability

The sequence variants in *SEPHS1* (NCBI ID 22929, transcript GenBank: NM_012247.4) reported in the paper have been deposited in ClinVar database (SCV002103293.1, SCV002103295.1, SCV002103294.2, SCV002103296.1) (https://www.ncbi.nlm.nih.gov/clinvar/) (Table 1). Exome sequencing data were generated in diagnostic setting and can not be shared due to privacy concerns.

Consortia

Members of the Undiagnosed Diseases Network are Maria T. Acosta, Margaret Adam, David R. Adams, Justin Alvey, Laura Amendola, Ashley Andrews, Euan A. Ashley, Mahshid S. Azamian, Carlos A. Bacino, Guney Bademci, Ashok Balasubramanyam, Dustin Baldridge, Jim Bale, Michael Bamshad, Deborah Barbouth, Pinar Bayrak-Toydemir, Anita Beck, Alan H. Beggs, Edward Behrens, Gill Bejerano, Hugo J. Bellen, Jimmy Bennet, Beverly Berg-Rood, Jonathan A. Bernstein, Gerard T. Berry, Anna Bican, Stephanie Bivona, Elizabeth Blue, John Bohnsack, Devon Bonner, Lorenzo Botto, Brenna Boyd, Lauren C. Briere, Elly Brokamp, Gabrielle Brown, Elizabeth A. Burke, Lindsay C. Burrage, Manish J. Butte, Peter Byers, William E. Byrd, John Carey, Olveen Carrasquillo, Thomas Cassini, Ta Chen Peter Chang, Sirisak Chanprasert, Hsiao-Tuan Chao, Gary D. Clark, Terra R. Coakley, Laurel A. Cobban, Joy D. Cogan, Matthew Coggins, F. Sessions Cole, Heather A. Colley, Cynthia M. Cooper, Heidi Cope, William J. Craigen, Andrew B. Crouse, Michael Cunningham, Precilla D'Souza, Hongzheng Dai, Surendra Dasari, Joie Davis, Jyoti G. Dayal, Matthew Deardorff, Esteban C. Dell'Angelica, Katrina Dipple, Daniel Doherty, Naghmeh Dorrani, Argenia L. Doss, Emilie D. Douine, Laura Duncan, Dawn Earl, David J. Eckstein, Lisa T. Emrick, Christine M. Eng, Cecilia Esteves, Marni Falk, Liliana Fernandez, Elizabeth L. Fieg, Paul G. Fisher, Brent L. Fogel, Irman Forghani, William A. Gahl, Ian Glass, Bernadette Gochuico, Rena A. Godfrey, Katie Golden-Grant, Madison P. Goldrich, Alana Grajewski, Irma Gutierrez, Don Hadley, Sihoun Hahn, Rizwan Hamid, Kelly Hassey, Nichole Hayes, Frances High, Anne Hing, Fuki M. Hisama, Ingrid A. Holm, Jason Hom, Martha Horike-Pyne, Alden Huang, Yong Huang, Wendy Introne, Rosario Isasi, Kosuke Izumi, Fariha Jamal, Gail P. Jarvik, Jeffrey Jarvik, Suman Jayadev, Orpa Jean-Marie, Vaidehi Jobanputra, Lefkothea Karaviti, Jennifer Kennedy, Shamika Ketkar, Dana Kiley, Gonench Kilich, Shilpa N. Kobren, Isaac S. Kohane, Jennefer N. Kohler, Deborah Krakow, Donna M. Krasnewich, Elijah Kravets, Susan Korrick, Mary Koziura, Seema R. Lalani, Byron Lam, Christina Lam, Grace L. LaMoure, Brendan C. Lanpher, Ian R. Lanza, Kimberly LeBlanc, Brendan H. Lee, Roy Levitt, Richard A. Lewis, Pengfei Liu, Xue Zhong Liu, Nicola Longo, Sandra K. Loo, Joseph Loscalzo, Richard L. Maas, Ellen F. Macnamara, Calum A. MacRae, Valerie V. Maduro, Rachel Mahoney, Bryan C. Mak, May Christine V. Malicdan, Laura A. Mamounas, Teri A. Manolio, Rong Mao, Kenneth Maravilla, Ronit Marom, Gabor Marth, Beth A. Martin, Martin G. Martin, Julian A. Martínez-Agosto, Shruti Marwaha, Jacob McCauley, Allyn McConkie-Rosell, Alexa T. McCray, Elisabeth McGee, Heather Mefford, J. Lawrence Merritt, Matthew Might, Ghayda Mirzaa, Eva Morava, Paolo M. Moretti, Mariko Nakano-Okuno, Stan F. Nelson, John H. Newman, Sarah K. Nicholas, Deborah Nickerson, Shirley Nieves-Rodriguez, Donna Novacic, Devin Oglesbee, James P. Orengo, Laura Pace, Stephen Pak, J. Carl Pallais, Christina GS. Palmer, Jeanette C. Papp, Neil H. Parker, John A. Phillips III, Jennifer E. Posey, Lorraine Potocki, Barbara N. Pusey, Aaron Quinlan, Wendy Raskind, Archana N. Raja, Deepak A. Rao, Anna Raper, Genecee Renteria, Chloe M. Reuter, Lynette Rives, Amy K. Robertson, Lance H. Rodan, Jill A. Rosenfeld, Natalie Rosenwasser, Francis Rossignol, Maura Ruzhnikov, Ralph Sacco, Jacinda B. Sampson, Mario Saporta, Judy Schaechter, Timothy Schedl, Kelly Schoch, C. Ron Scott, Daryl A. Scott, Vandana Shashi, Jimann Shin, Edwin K. Silverman, Janet S. Sinsheimer, Kathy Sisco, Edward C. Smith, Kevin S. Smith, Emily Solem, Lilianna Solnica-Krezel, Ben Solomon, Rebecca C. Spillmann, Joan M. Stoler, Jennifer A. Sullivan, Kathleen Sullivan, Angela Sun, Shirley Sutton, David A. Sweetser, Virginia Sybert, Holly K. Tabor, Amelia L. M. Tan, Queenie K.-G. Tan, Mustafa Tekin, Fred Telischi, Willa Thorson, Cynthia J. Tifft, Camilo Toro, Alyssa A. Tran, Brianna M. Tucker, Tiina K. Urv, Adeline Vanderver, Matt Velinder, Dave Viskochil, Tiphanie P. Vogel, Colleen E. Wahl, Melissa Walker, Stephanie Wallace, Nicole M. Walley, Jennifer Wambach, Jijun Wan, Lee-kai Wang, Michael F. Wangler, Patricia A. Ward, Daniel Wegner, Monika Weisz-Hubshman, Mark Wener, Tara Wenger, Katherine Wesseling Perry, Monte Westerfield, Matthew T. Wheeler, Jordan Whitlock, Lynne A. Wolfe, Kim Worley, Changrui Xiao, Shinya Yamamoto, John Yang, Diane B. Zastrow, Zhe Zhang, Chunli Zhao, Stephan Zuchner.

Supplemental information

Supplemental information can be found online at https://doi.org/10.1016/j.ajhg.2024.02.016.

Acknowledgments

We would like to thank all the families for participating in this study. This work was in part supported by The National Institute of General Medical Sciences, National Institutes of Health grant GM097042 (to M.S.). Research reported in this manuscript was supported by the NIH Common Fund, through the Office of

Strategic Coordination/Office of the NIH Director under Award Number(s) [U01HG010233]. The content is solely the responsibility of the authors and does not necessarily represent the official views of the National Institutes of Health.

Declaration of interests

S.V.M., E.T., H.G., T.B.P., A.T., D.A.C., M.M.M., I.M.W., K.G.M., and J.J. are employees of GeneDx., LLC. This article was prepared while M.S. was employed at the University of Illinois at Chicago. The opinions expressed in this article are the author's own and do not reflect the view of the National Institutes of Health, the Department of Health and Human Services, or the United States government.

Received: April 4, 2023
Accepted: February 28, 2024
Published: March 25, 2024

Web resources

Clustal Omega, https://www.ebi.ac.uk/Tools/msa/clustalo/
DGV, http://dgv.tcag.ca/dgv/app/home.
GeneMatcher, https://genematcher.org/
gnomAD, https://gnomad.broadinstitute.org/
MetaDome, https://stuart.radboudumc.nl/metadome/
OMIM, https://www.omim.org/
The Human Protein Atlas, https://www.proteinatlas.org/
PROVEAN, http://provean.jcvi.org/

References

1. Cardoso, B.R., Cominetti, C., and Seale, L.A. (2021). Editorial: Selenium, Human Health and Chronic Disease. Front. Nutr. *8*, 827759. https://doi.org/10.3389/fnut.2021.827759.
2. Hilal, T., Killam, B.Y., Grozdanović, M., Dobosz-Bartoszek, M., Loerke, J., Bürger, J., Mielke, T., Copeland, P.R., Simonović, M., and Spahn, C.M.T. (2022). Structure of the mammalian ribosome as it decodes the selenocysteine UGA codon. Science *376*, 1338–1343. https://doi.org/10.1126/science.abg3875.
3. Palioura, S., Sherrer, R.L., Steitz, T.A., Söll, D., and Simonovic, M. (2009). The human SepSecS-tRNASec complex reveals the mechanism of selenocysteine formation. Science *325*, 321–325. https://doi.org/10.1126/science.1173755.
4. Xu, X.M., Carlson, B.A., Mix, H., Zhang, Y., Saira, K., Glass, R.S., Berry, M.J., Gladyshev, V.N., and Hatfield, D.L. (2007). Biosynthesis of selenocysteine on its tRNA in eukaryotes. PLoS Biol. *5*, e4. https://doi.org/10.1371/journal.pbio.0050004.
5. Yuan, J., Palioura, S., Salazar, J.C., Su, D., O'Donoghue, P., Hohn, M.J., Cardoso, A.M., Whitman, W.B., and Söll, D. (2006). RNA-dependent conversion of phosphoserine forms selenocysteine in eukaryotes and archaea. Proc. Natl. Acad. Sci. USA *103*, 18923–18927. https://doi.org/10.1073/pnas.0609703104.
6. Bellinger, F.P., Raman, A.V., Rueli, R.H., Bellinger, M.T., Dewing, A.S., Seale, L.A., Andres, M.A., Uyehara-Lock, J.H., White, L.R., Ross, G.W., and Berry, M.J. (2012). Changes in selenoprotein P in substantia nigra and putamen in Parkinson's disease. J. Parkinsons Dis. *2*, 115–126. https://doi.org/10.3233/JPD-2012-11052.
7. Pillai, R., Uyehara-Lock, J.H., and Bellinger, F.P. (2014). Selenium and selenoprotein function in brain disorders. IUBMB Life *66*, 229–239. https://doi.org/10.1002/iub.1262.
8. Berry, M.J., Banu, L., Chen, Y.Y., Mandel, S.J., Kieffer, J.D., Harney, J.W., and Larsen, P.R. (1991). Recognition of UGA as a selenocysteine codon in type I deiodinase requires sequences in the 3′ untranslated region. Nature *353*, 273–276. https://doi.org/10.1038/353273a0.
9. Boukhzar, L., Hamieh, A., Cartier, D., Tanguy, Y., Alsharif, I., Castex, M., Arabo, A., El Hajji, S., Bonnet, J.J., Errami, M., et al. (2016). Selenoprotein T Exerts an Essential Oxidoreductase Activity That Protects Dopaminergic Neurons in Mouse Models of Parkinson's Disease. Antioxidants Redox Signal. *24*, 557–574. https://doi.org/10.1089/ars.2015.6478.
10. Schoenmakers, E., and Chatterjee, K. (2021). Human Genetic Disorders Resulting in Systemic Selenoprotein Deficiency. Int. J. Mol. Sci. *22*, 12927. https://doi.org/10.3390/ijms222312927.
11. Puppala, A.K., French, R.L., Matthies, D., Baxa, U., Subramaniam, S., and Simonović, M. (2016). Structural basis for early-onset neurological disorders caused by mutations in human selenocysteine synthase. Sci. Rep. *6*, 32563. https://doi.org/10.1038/srep32563.
12. Dumitrescu, A.M., Liao, X.H., Abdullah, M.S.Y., Lado-Abeal, J., Majed, F.A., Moeller, L.C., Boran, G., Schomburg, L., Weiss, R.E., and Refetoff, S. (2005). Mutations in SECISBP2 result in abnormal thyroid hormone metabolism. Nat. Genet. *37*, 1247–1252. https://doi.org/10.1038/ng1654.
13. Shao, Z.Q., Zhang, X., Fan, H.H., Wang, X.S., Wu, H.M., Zhang, L., Cheng, W.H., and Zhu, J.H. (2019). Selenoprotein T Promotes Proliferation and G1-to-S Transition in SK-N-SH Cells: Implications in Parkinson's Disease. J. Nutr. *149*, 2110–2119. https://doi.org/10.1093/jn/nxz199.
14. Ben-Zeev, B., Hoffman, C., Lev, D., Watemberg, N., Malinger, G., Brand, N., and Lerman-Sagie, T. (2003). Progressive cerebellocerebral atrophy: a new syndrome with microcephaly, mental retardation, and spastic quadriplegia. J. Med. Genet. *40*, e96. https://doi.org/10.1136/jmg.40.8.e96.
15. Çatli, G., Fujisawa, H., Kirbiyik, Ö., Mimoto, M.S., Gençpinar, P., Özdemir, T.R., Dündar, B.N., and Dumitrescu, A.M. (2018). A Novel Homozygous Selenocysteine Insertion Sequence Binding Protein 2 (SECISBP2, SBP2) Gene Mutation in a Turkish Boy. Thyroid *28*, 1221–1223. https://doi.org/10.1089/thy.2018.0015.
16. Schoenmakers, E., Carlson, B., Agostini, M., Moran, C., Rajanayagam, O., Bochukova, E., Tobe, R., Peat, R., Gevers, E., Muntoni, F., et al. (2016). Mutation in human selenocysteine transfer RNA selectively disrupts selenoprotein synthesis. J. Clin. Invest. *126*, 992–996. https://doi.org/10.1172/JCI84747.
17. Geslot, A., Savagner, F., and Caron, P. (2021). Inherited Selenocysteine Transfer RNA Mutation: Clinical and Hormonal Evaluation of 2 Patients. Eur. Thyroid J. *10*, 542–547. https://doi.org/10.1159/000518275.
18. Pavlidou, E., Salpietro, V., Phadke, R., Hargreaves, I.P., Batten, L., McElreavy, K., Pitt, M., Mankad, K., Wilson, C., Cutrupi, M.C., et al. (2016). Pontocerebellar hypoplasia type 2D and optic nerve atrophy further expand the spectrum associated with selenoprotein biosynthesis deficiency. Eur. J. Paediatr. Neurol. *20*, 483–488. https://doi.org/10.1016/j.ejpn.2015.12.016.
19. Kang, D., Lee, J., Jung, J., Carlson, B.A., Chang, M.J., Chang, C.B., Kang, S.B., Lee, B.C., Gladyshev, V.N., Hatfield, D.L.,

et al. (2022). Selenophosphate synthetase 1 deficiency exacerbates osteoarthritis by dysregulating redox homeostasis. Nat. Commun. *13*, 779. https://doi.org/10.1038/s41467-022-28385-7.

20. Na, J., Jung, J., Bang, J., Lu, Q., Carlson, B.A., Guo, X., Gladyshev, V.N., Kim, J., Hatfield, D.L., and Lee, B.J. (2018). Selenophosphate synthetase 1 and its role in redox homeostasis, defense and proliferation. Free Radic. Biol. Med. *127*, 190–197. https://doi.org/10.1016/j.freeradbiomed.2018.04.577.
21. Sjöstedt, E., Zhong, W., Fagerberg, L., Karlsson, M., Mitsios, N., Adori, C., Oksvold, P., Edfors, F., Limiszewska, A., Hikmet, F., et al. (2020). An atlas of the protein-coding genes in the human, pig, and mouse brain. Science *367*, eaay5947. https://doi.org/10.1126/science.aay5947.
22. Tobe, R., Carlson, B.A., Huh, J.H., Castro, N.P., Xu, X.-M., Tsuji, P.A., Lee, S.-G., Bang, J., Na, J.-W., Kong, Y.-Y., et al. (2016). Selenophosphate synthetase 1 is an essential protein with roles in regulation of redox homoeostasis in mammals. Biochem. J. *473*, 2141–2154. https://doi.org/10.1042/bcj20160393.
23. Bang, J., Han, M., Yoo, T.-J., Qiao, L., Jung, J., Na, J., Carlson, B.A., Gladyshev, V.N., Hatfield, D.L., Kim, J.-H., et al. (2021). Identification of Signaling Pathways for Early Embryonic Lethality and Developmental Retardation in Sephs1−/− Mice. Int. J. Mol. Sci. *22*, 11647.
24. Jung, J., Kim, Y., Na, J., Qiao, L., Bang, J., Kwon, D., Yoo, T.-J., Kang, D., Kim, L.K., Carlson, B.A., et al. (2021). Constitutive Oxidative Stress by SEPHS1 Deficiency Induces Endothelial Cell Dysfunction. Int. J. Mol. Sci. *22*, 11646.
25. Tobe, R., Carlson, B.A., Huh, J.H., Castro, N.P., Xu, X.M., Tsuji, P.A., Lee, S.G., Bang, J., Na, J.W., Kong, Y.Y., et al. (2016). Selenophosphate synthetase 1 is an essential protein with roles in regulation of redox homoeostasis in mammals. Biochem. J. *473*, 2141–2154. https://doi.org/10.1042/BCJ20160393.
26. Shim, M.S., Kim, J.Y., Jung, H.K., Lee, K.H., Xu, X.M., Carlson, B.A., Kim, K.W., Kim, I.Y., Hatfield, D.L., and Lee, B.J. (2009). Elevation of glutamine level by selenophosphate synthetase 1 knockdown induces megamitochondrial formation in Drosophila cells. J. Biol. Chem. *284*, 32881–32894. https://doi.org/10.1074/jbc.M109.026492.
27. Qiao, L., Dho, S.H., Kim, J.Y., and Kim, L.K. (2022). SEPHS1 is dispensable for pluripotency maintenance but indispensable for cardiac differentiation in mouse embryonic stem cells. Biochem. Biophys. Res. Commun. *590*, 125–131. https://doi.org/10.1016/j.bbrc.2021.12.091.
28. Sobreira, N., Schiettecatte, F., Valle, D., and Hamosh, A. (2015). GeneMatcher: a matching tool for connecting investigators with an interest in the same gene. Hum. Mutat. *36*, 928–930. https://doi.org/10.1002/humu.22844.
29. Rots, D., Chater-Diehl, E., Dingemans, A.J.M., Goodman, S.J., Siu, M.T., Cytrynbaum, C., Choufani, S., Hoang, N., Walker, S., Awamleh, Z., et al. (2021). Truncating SRCAP variants outside the Floating-Harbor syndrome locus cause a distinct neurodevelopmental disorder with a specific DNA methylation signature. Am. J. Hum. Genet. *108*, 1053–1068. https://doi.org/10.1016/j.ajhg.2021.04.008.
30. Huang, N., Lee, I., Marcotte, E.M., and Hurles, M.E. (2010). Characterising and predicting haploinsufficiency in the human genome. PLoS Genet. *6*, e1001154. https://doi.org/10.1371/journal.pgen.1001154.
31. MacDonald, J.R., Ziman, R., Yuen, R.K.C., Feuk, L., and Scherer, S.W. (2014). The Database of Genomic Variants: a curated collection of structural variation in the human genome. Nucleic Acids Res. *42*, D986–D992. https://doi.org/10.1093/nar/gkt958.
32. Wiel, L., Baakman, C., Gilissen, D., Veltman, J.A., Vriend, G., and Gilissen, C. (2019). MetaDome: Pathogenicity analysis of genetic variants through aggregation of homologous human protein domains. Hum. Mutat. *40*, 1030–1038. https://doi.org/10.1002/humu.23798.
33. Richards, C.S., Bale, S., Bellissimo, D.B., Das, S., Grody, W.W., Hegde, M.R., Lyon, E., Ward, B.E.; and Molecular Subcommittee of the ACMG Laboratory Quality Assurance Committee (2008). ACMG recommendations for standards for interpretation and reporting of sequence variations: Revisions 2007. Genet. Med. *10*, 294–300. https://doi.org/10.1097/GIM.0b013e31816b5cae.
34. Zhang, Y., Zhou, Y., Schweizer, U., Savaskan, N.E., Hua, D., Kipnis, J., Hatfield, D.L., and Gladyshev, V.N. (2008). Comparative analysis of selenocysteine machinery and selenoproteome gene expression in mouse brain identifies neurons as key functional sites of selenium in mammals. J. Biol. Chem. *283*, 2427–2438. https://doi.org/10.1074/jbc.M707951200.
35. van Trotsenburg, P., Stoupa, A., Léger, J., Rohrer, T., Peters, C., Fugazzola, L., Cassio, A., Heinrichs, C., Beauloye, V., Pohlenz, J., et al. (2021). Congenital Hypothyroidism: A 2020-2021 Consensus Guidelines Update-An ENDO-European Reference Network Initiative Endorsed by the European Society for Pediatric Endocrinology and the European Society for Endocrinology. Thyroid *31*, 387–419. https://doi.org/10.1089/thy.2020.0333.
36. Marr, A., Yokubynas, N., Tang, K., Saleh, D., Wherrett, D.K., Stein, R., Bassilious, E., Chakraborty, P., and Lawrence, S.E. (2022). Transient vs Permanent Congenital Hypothyroidism in Ontario, Canada: Predictive Factors and Scoring System. J. Clin. Endocrinol. Metab. *107*, 638–648. https://doi.org/10.1210/clinem/dgab798.
37. Santesmasses, D., Mariotti, M., and Gladyshev, V.N. (2020). Bioinformatics of Selenoproteins. Antioxidants Redox Signal. *33*, 525–536. https://doi.org/10.1089/ars.2020.8044.
38. Hebron, K.E., Hernandez, E.R., and Yohe, M.E. (2022). The RASopathies: from pathogenetics to therapeutics. Dis. Model. Mech. *15*, dmm049107. https://doi.org/10.1242/dmm.049107.

The American Journal of Human Genetics, Volume *111*

Supplemental information

De novo missense variants in exon 9 of *SEPHS1* cause a neurodevelopmental condition with developmental delay, poor growth, hypotonia, and dysmorphic features

Sureni V. Mullegama, Kaitlyn A. Kiernan, Erin Torti, Ethan Pavlovsky, Nicholas Tilton, Austin Sekula, Hua Gao, Joseph T. Alaimo, Kendra Engleman, Eric T. Rush, Karli Blocker, Katrina M. Dipple, Veronica M. Fettig, Heather Hare, Ian Glass, Dorothy K. Grange, Michael Griffin, Chanika Phornphutkul, Lauren Massingham, Lakshmi Mehta, Danny E. Miller, Jenny Thies, J Lawrence Merritt II, Eric Muller II, Matthew Osmond, Sarah L. Sawyer, Rachel Slaugh, Rachel E. Hickey, Barry Wolf, Care4Rare Canada Consortium, Undiagnosed Diseases Network, Sanjeev Choudhary, Miljan Simonović, Yueqing Zhang, Timothy Blake Palculict, Aida Telegrafi, Deanna Alexis Carere, Ingrid M. Wentzensen, Michelle M. Morrow, Kristin G. Monaghan, Jun Yang, and Jane Juusola

Supplemental Information

Supplement Note: Considerations for care of patients with *SEPHS1* variants

Individuals with pathogenic variants in *SEPHS1* appear to have a neurodevelopmental and growth disorder, with variable effects on other body systems. Considerations for immediate and long-term care of these individuals might include:

1. Frequent assessment of developmental milestones, with targeted interventions as needed
2. Psychoeducational evaluation in school-age children
3. Screening for neurobehavioral concerns, including attention-deficit/hyperactivity disorder and obsessive-compulsive disorder.
4. Screening for neurologic and muscular concerns with low threshold for referral to a specialist
5. Monitoring of height and weight
6. Feeding evaluation
7. Screening for endocrine abnormalities, including hypocalcemia, Hasimoto's thyroiditis, elevated B6, growth hormone deficiency. It is unknown if this needs to be followed over time
8. Eye examination
9. Sleep study

A

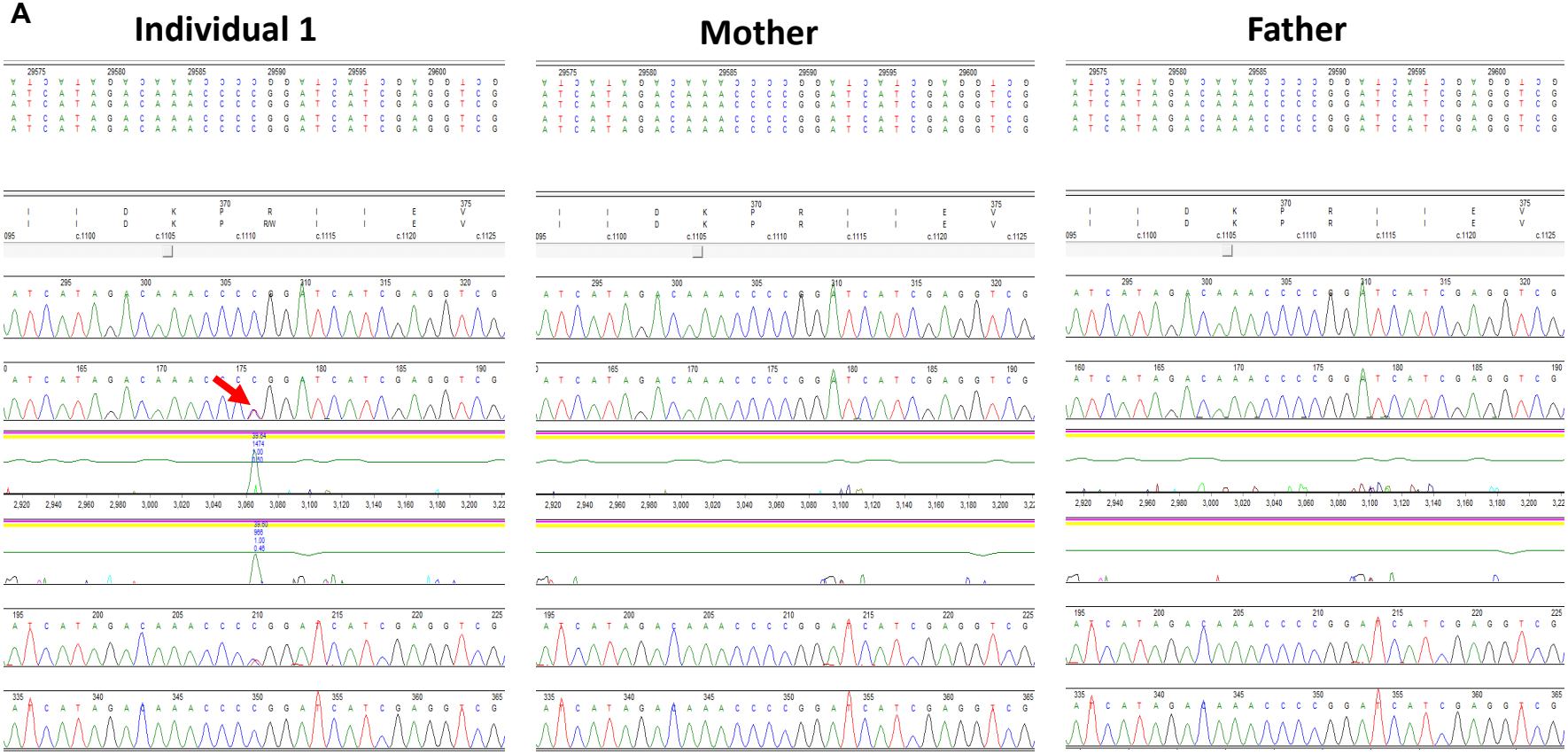

B

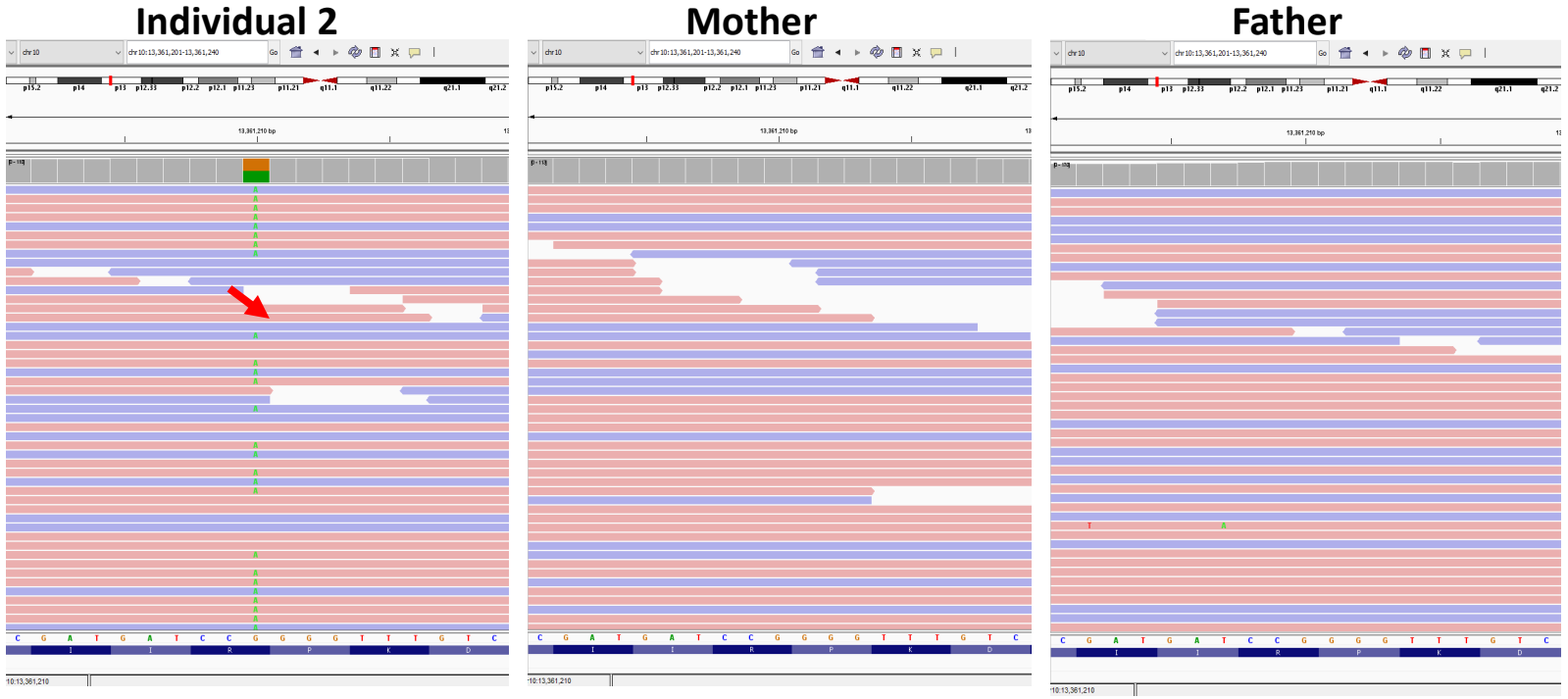

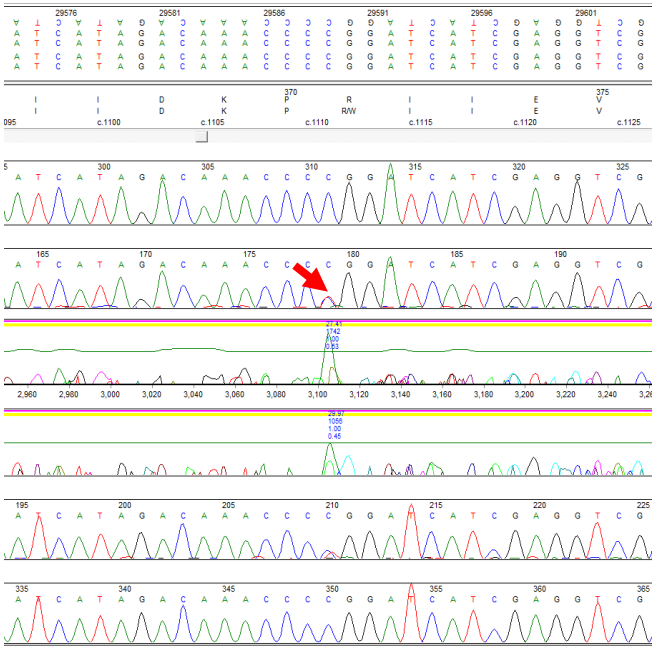

Mother & Father

No ABI data (high quality NGS, no confirmation)

C

Individual 3

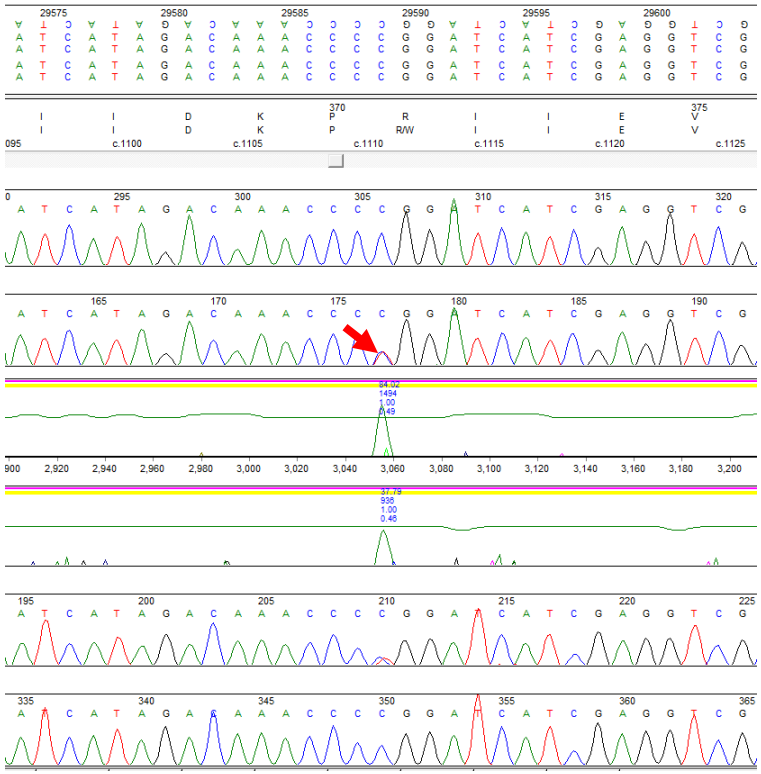

D

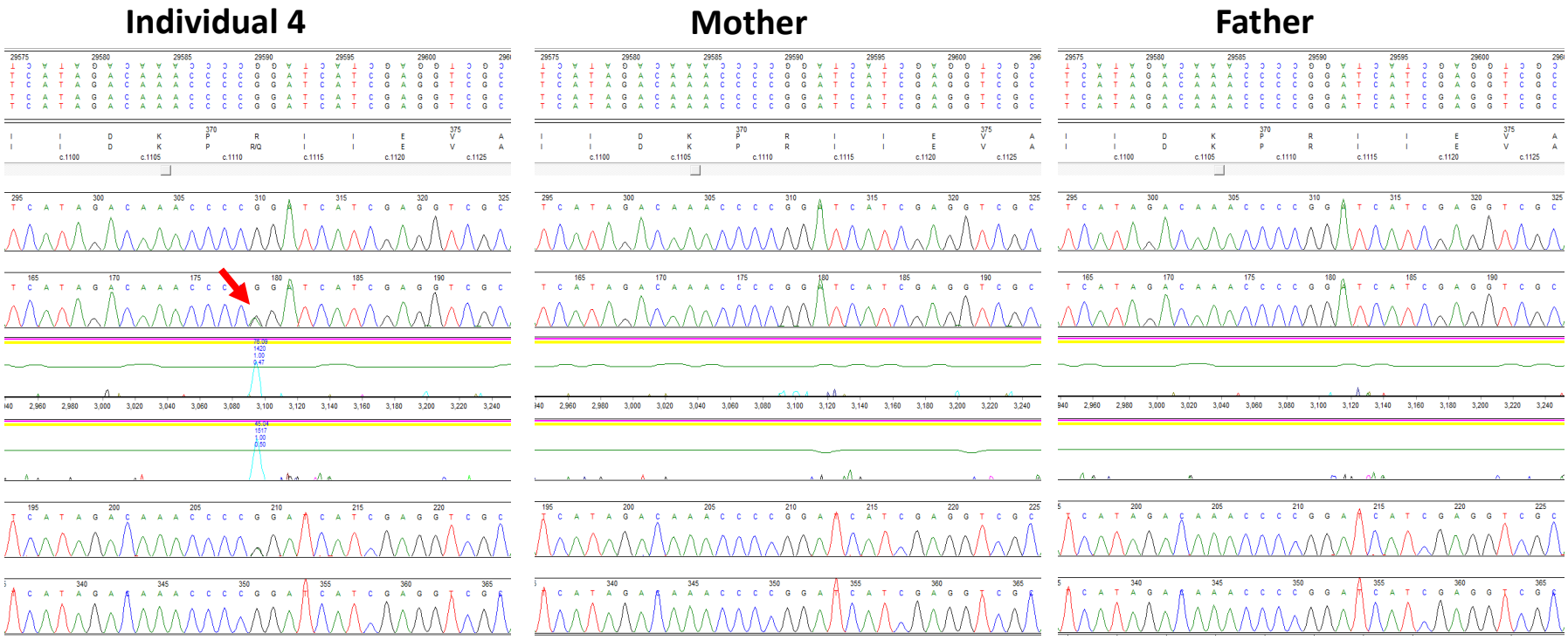

E

Individual 6

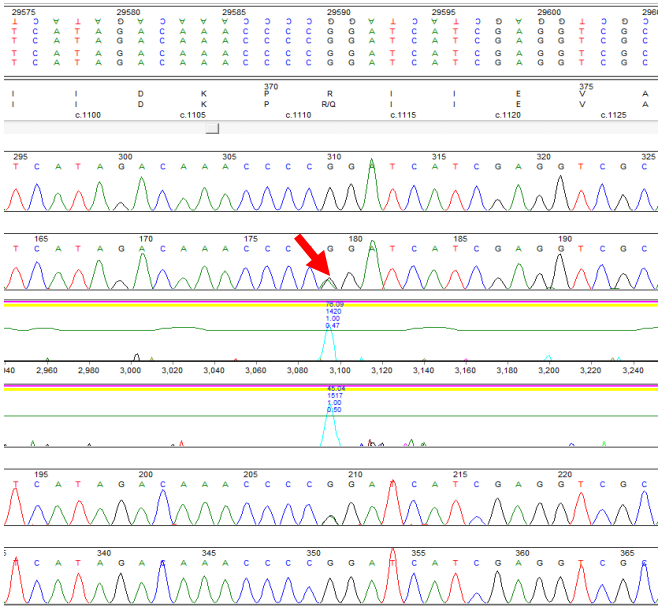

Mother

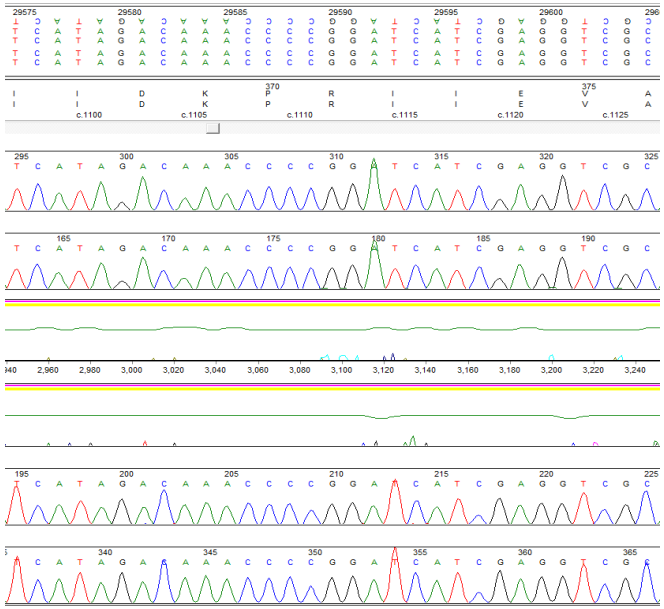

Father

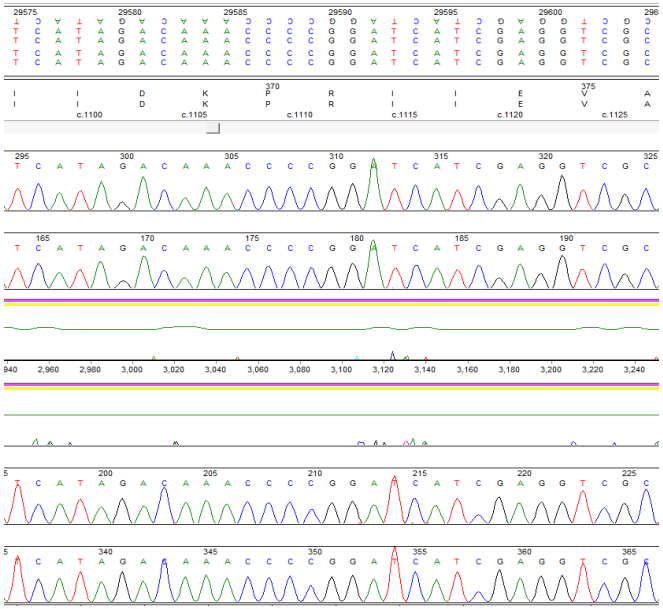

F

Individual 7

Mother

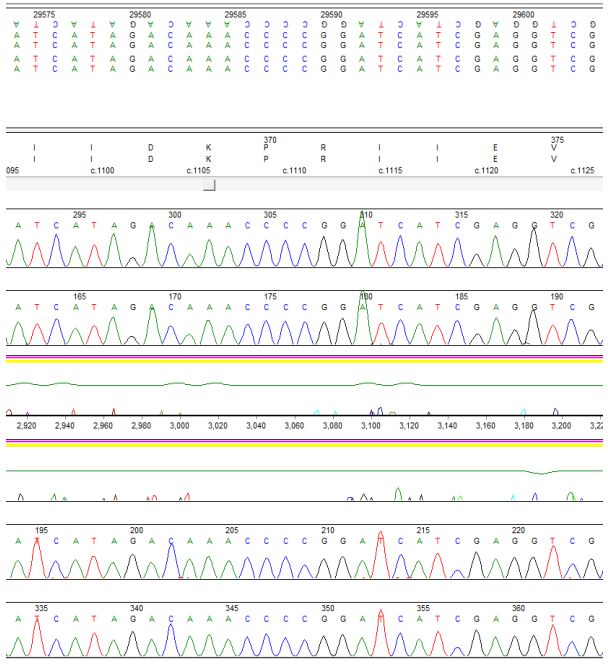

Father

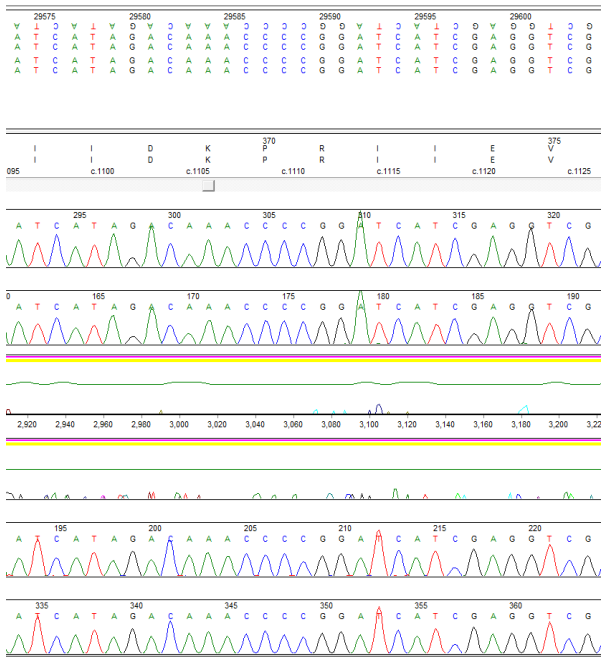

G

Individual 8

H

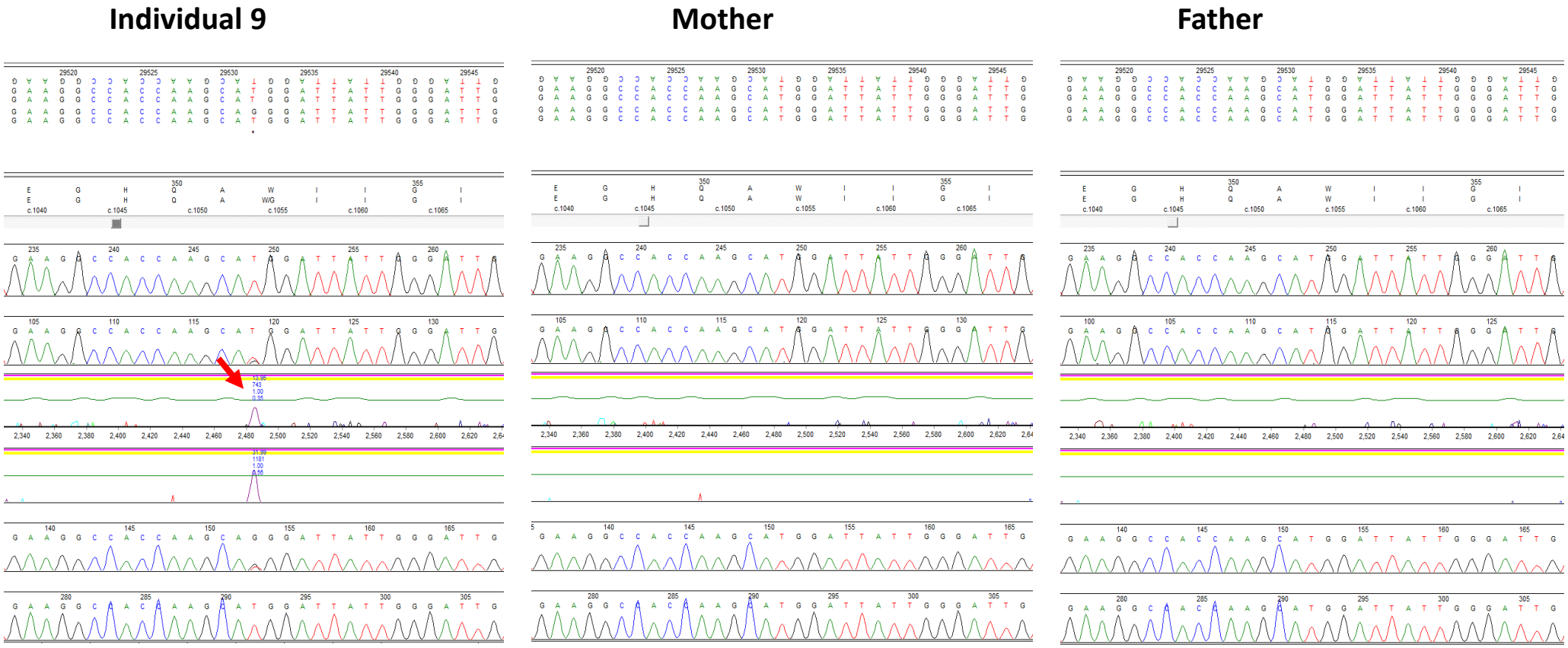

Figure S1. Sequence traces of all available individuals with variants in *SEPHS1* and their available parents (A-H). (A) Individual 1; *SEPHS1*, NM_012247.4: c.1111C>T, Arg371Trp (B) Individual 2*; SEPHS1*, NM_012247.4: c.1111C>T, Arg371Trp (C) Individual 3; *SEPHS1*, NM_012247.4: c.1111C>T, Arg371Trp (D) Individual 4; *SEPHS1*, NM_012247.4: c.1112G>A, p.Arg371Gln (E) Individual 6; *SEPHS1*, NM_012247.4: c.1112G>A, p.Arg371Gln (F) Individual 7; *SEPHS1*, NM_012247.4: c.1111C>G, p.Arg371Gly (G) Individual 8; *SEPHS1*, NM_012247.4: c.1111C>G, p.Arg371Gly (H) *SEPHS1*, NM_012247.4: c.1054T>G, p.Trp352Gly

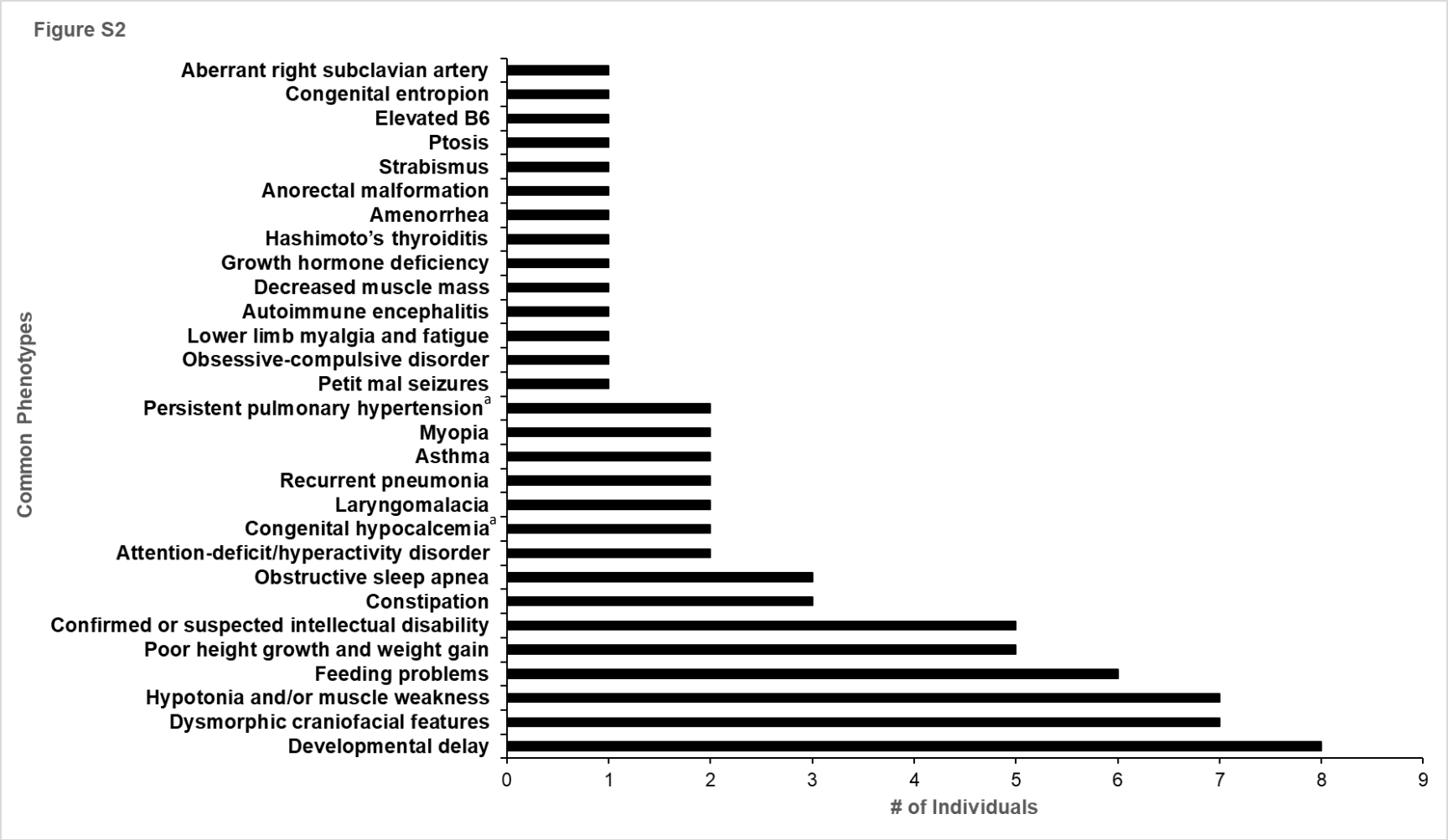

Figure S2. Phenotypes present in individuals with *SEPHS1* variants

[a]These individuals are siblings.

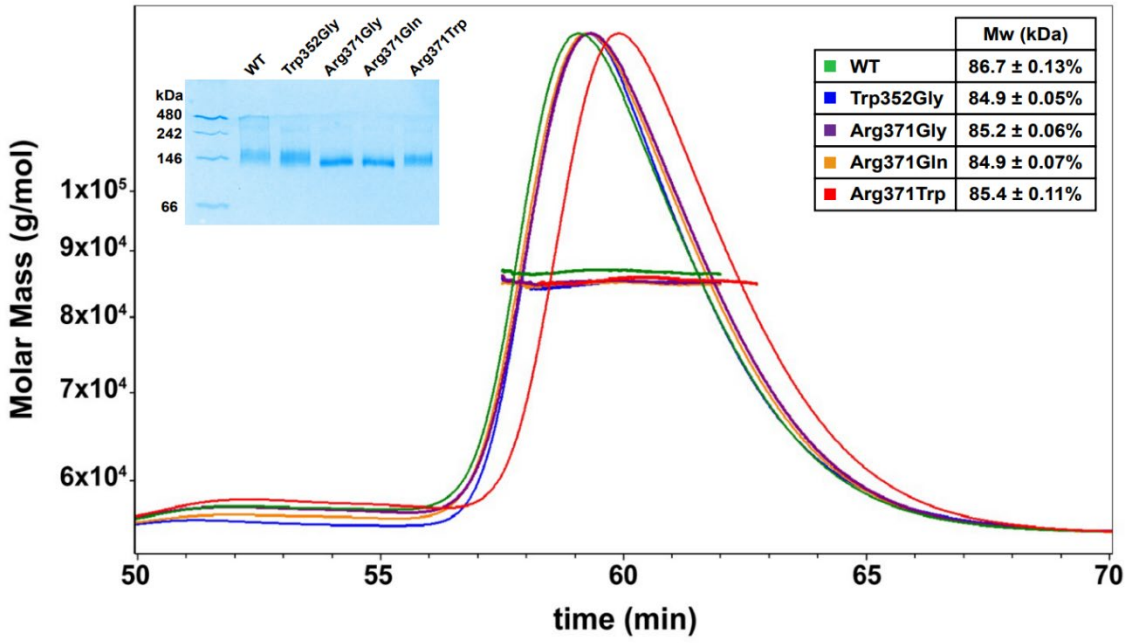

Figure S3. Native-PAGE and SEC-MALS of SEPHS1 samples. **Figure S3. Native-PAGE and SEC-MALS of SEPHS1 samples.** Accurate molecular weight and size was determined for WT, Trp352Gly, Arg371Gly, Arg371Gln, and Arg371Trp. Light scattering curves are plotted against time and molecular weight is plotted across each peak. All samples had an average polydispersity of 1.0 ± 0.001%.

	Individual 1	Individual 2	Individual 3	Individual 4	Individual 5	Individual 6	Individual 9
Eyes		Deep set palpebral fissures with mild asymmetry	Deep set eyes, dark and thick lashes, horizontal palpebral fissures		Heavy eyebrows with a lateral flare	Long lashes, ptosis	Mildly arched eyebrows with long lashes; entropion; bilateral ptosis requiring surgery
Ears	Cupped, asymmetric, low set, hypoplastic with bilateral preauricular pits		Small, cupped	Mildly dysplastic, thick helix, Stahl's Ear	Ears are small with poor development of the superior helix	Low set, cupped, fleshy helices	
Nose	Broad nasal root			Slightly prominent nose	Prominent nasal bridge, nasal turbinate reduction	Overhanging columella	Mildly bulbous nasal tip
Mouth	Ankyloglossia	Ankyloglossia	Small widely spaced teeth	Mild bifid uvula	Ankyloglossia; thin vermillion	Abnormal philtrum, thin lips	Ankyloglossia

Table S1. Description of facial features of the seven individuals

Target	Forward (5’ - 3’)	Reverse (5’ - 3’)
GPX1	CAG TCG GTG TAT GCC TTC TC	GCT CGT TCA TCT GGG TGT AG
MSRB1	CAC ACT GTC GGC TGA CTT AG	GAG GGT GTA ACG TCA TTC AGA G
SELENOW	TCC AGG TGG GAG GTT AGT	CCT CAA GCG CCA CAA TAA AC
SELENOT	CGT GCC CAG CAA GAG ATT A	CCG CAT GTA CTC CTC AAA CA
GSTO1	TCA TCT GGC CCT GGT TTG	GCT GAG ACT GTG GGA TCT TC
PRDX1	CCC ACG GAG ATC ATT GCT T	GTC CCA GTC CTC CTT GTT TC
GSTA4	CCC GAA GCA TTC TCC ACT AC	CCC TCC ACG TAC ATG TCA ATC
SOD3	AGG TCT CAC CTT CGC CTT TG	TCA GAC CTA CTG AGT GGG GG
PolB	ACC GAC ATG CTC ACA GAA C	AGC TTC AGC TCC ACT CTT TAT T

Table S2. Real-Time Quantitative Reverse Transcription PCR primer sequences for mRNA expression analysis

Materials and Methods

IRB

This study was conducted under GeneDx's research protocol ''Research to Expand the Understanding of Genetic Variants: Clinical and Genetic Correlations", approved by the Western Institutional Review Board (IRB) (protocol 20171030). All research subjects provided written consent to participate through either GeneDx's research protocol or as required by their clinical institution.

Exome Sequencing

For Individuals 1-4 and 7-9, we used genomic DNA from the proband, parents and affected sibling (when available). The exonic regions and flanking splice junctions of the genome were captured using the IDT xGen Exome Research Panel v1.0 (Integrated DNA Technologies, Coralville, IA). Massively parallel (NextGen) sequencing was done on an Illumina system with 100bp or greater paired-end reads. Reads were aligned to human genome build GRCh37/UCSC hg19, and analyzed for sequence variants using a custom-developed analysis tool. Reported variants were confirmed, if necessary, by an appropriate orthogonal method in the proband and, if submitted, in selected relatives. Additional sequencing technology and variant interpretation protocol has been previously described[1]. The general assertion criteria for variant classification are publicly available on the GeneDx ClinVar submission page (http://www.ncbi.nlm.nih.gov/clinvar/submitters/26957/)

For Individual 5, exome sequencing was performed as previously described[2]. Briefly, Whole exome sequencing (WES) is performed using genomic DNA from the submitted sample, prepared using the Kapa or TruSeq library prep. Samples are enriched using IDT xGen exome research panel v 1.0 and sequenced to a minimum of 7 Gb of 2x125 paired end reads for a mean of 80x average coverage or greater on the Illumina NOVA Seq. Bidirectional sequence is assembled, aligned to reference gene sequences based on human genome build GRCh37/UCSC hg19, and analyzed using custom-developed software.

Individual 6 used genomic DNA from the proband and unaffected parents. Exonic DNA was selected using the xGen Exome Research Panel with custom-designed capture probes (Integrated DNA Technologies, Coralville, IA). Sequencing was performed using the Illumina sequencing system with 2 x 150bp chemistry. Read alignment, variant calling, annotation, and analysis of sequencing data were done as outlined for previous FORGE and Care4Rare Canada projects [3].

Plasmid Construction

The *SEPHS1* was cloned from plasmid pANT7-SEPHS1, a kind gift from Dr. Christian Baron from the University of Montreal. The *SEPHS1* coding sequence was inserted into the pET15b expression vector (Novagen 69661) to generate pET15b-SPS1. Site-

directed mutagenesis was performed on pET15b-SPS1 to generate expression plasmids for each mutant (Trp352Gly, Arg371Gly, Arg371Gln, Arg371Trp).

Protein Expression and Purification

Recombinant SEPHS1 possessing an N-terminal 6xHis tag was produced in *E. coli* strain OverExpress C41(DE3) (Sigma-Aldrich). Cells were grown at +37ºC shaking until reaching an OD_{600} ~0.6-0.8. To induce protein expression, isopropyl B-D-1-thiogalactopyranoside (IPTG) was added to a final concentration of 0.5mM. All proteins were produced for 18 hours at +18ºC shaking at 180 rpm. Cells were then pelleted and resuspended in lysis buffer (50mM HEPES pH 7.5, 300mM NaCl, 1mM DTT, 5% glycerol) containing an EDTA-free protease inhibitor tablet (Roche). Cells were lysed via sonication on ice and the cell lysate was clarified at 27,000*g* for 45min at +4ºC. Clarified lysate was loaded directly onto a His-Trap FF Crude 5 mL column (Cytiva) and washed with lysis buffer containing 20mM imidazole. Recombinant SEPHS1 was eluted from the column with lysis buffer containing 350mM imidazole. Samples were further purified by size-exclusion chromatography (SEC) using a Superose 6 Increase 10/300 column GL (Cytiva). Fractions containing SEPHS1 were pooled and concentrated in storage buffer (20 mM HEPES pH 7.5, 200mM NaCl, 0.5mM TCEP, 5% Glycerol). Final samples were flash-frozen in liquid nitrogen and stored at -80ºC.

Native PAGE

For each SEPHS1 protein, 2µg of recombinant protein was loaded onto a 4% stacking and 10% resolving non-denaturing polyacrylamide gel. Gels were run in the NativePage Cathode Buffer (Invitrogen). Gels were stained with Coomassie R-250, destained, and imaged with the Gel Doc XR+ system (Bio-Rad).

ATPase Assay

Reactions were set up as follows: 15 µM SEPHS1, 50mM HEPES-KOH pH 7.5, 50mM KCl, 5mM MgCl2, 1mM DTT, 1mM ATP. Reactions were incubated at 37°C for 18 hours. ATP availability was measured at 0, 3, 6, and 18 hours. Reactions were stopped by heat denaturation, centrifuged at 16,000*g*, and either used immediately in the assay or flash frozen and stored at -80°C. ATP was quantified using the CellTiterGlo 2.0 assay kit (Promega). Samples were diluted 1000-fold and 100µL of diluted sample was added to 100µL of CellTiter-Glo Reagent in opaque white 96-well plates. The plate was incubated for 10 minutes at room temperature and measured in the FLUOstar Omega plate reader (BMG Labtech). ATP standards were prepared from 1pM - 10 µM to generate a standard curve. Total ATP concentration was interpolated from the generated standard curve.

Thermal Shift Assays

Initial fluorescence values and thermal unfolding profiles of recombinant SEPHS1 samples were measured using the Tycho NT.6 (Nanotemper). Total initial fluorescence was calculated using the combined sample fluorescence at 260nm and 280nm. Thermal unfolding profiles were generated by monitoring the change in fluorescence at 260nm and 280nm while samples were gradually heated up to 95°C. Normalized fluorescence (260nm) was plotted against temperature to generate the final curves. Melting temperature was determined using the inflection point of each profile. Data analysis was performed in GraphPad Prism version 9.2.0 (GraphPad Software, San Diego, California USA, www.graphpad.com). Statistical significance between samples was determined using one-way ANOVA followed by Tukey's multiple comparisons test.

Limited Proteolysis

Proteolysis was carried out in SEPHS1 storage buffer using recombinant SEPHS1 samples at a final concentration of 0.5mg/ml. Trypsin or Chymotrypsin proteases were added to the reactions at a final concentration of 10 ug/ml. Reactions were incubated for 30 minutes at 30°C for trypsin and 37°C for chymotrypsin. 2µg of total digested protein was analyzed with SDS-PAGE using 4-20% TGX precast gels (Bio-Rad). Gels were imaged with the Imager 2000 (Bio-Rad).

Size-Exclusion Chromatography with Multi-Angle Light Scattering (SEC-MALS)

SEC was performed in SEPHS1 storage buffer without glycerol where 250µL of recombination SEPHS1 at 1mg/ml was injected into the HPLC system (Shimadzu) and run over a Superdex s200 Increase 10/300 GL column (Cytiva). Directly following SEC, molecular weight was determined using the DAWN multi-angle light scattering (MALS) detector in combination with the OptiLab dRI detector (Wyatt Technology). Baseline detection, signal alignment, peak picking, and molecular weight determination was performed using Astra 8.0 (Wyatt Technology).

Cell Culture

Human neuroblastoma SH-SY5Y cells were obtained from American Type Culture Collection (ATCC, CRL-2266) and grown in DMEM containing 10% FBS, 1% penicillin/streptomycin in a humidified 5% CO_2 incubator at 37ºC.

Lentivirus-mediated Gene Overexpression

The 3XFLAG tagged *SEPHS1* cDNA of wild type and mutants were PCR amplified and cloned into the XbaI/EcoRI sites of lentivirus expression vector pLV-tetO-CMV-SV40-PuroLoxP through Gibson assembly, as previously described [4]. To produce infectious lentivirus, each construct was transfected into 293FT packaging cells together with the

lentiviral packaging plasmids using lipofectamine 2000 (Invitrogen). The empty vector was used as a negative control. The 293FT cells were cultured for 48 h and the virus-containing medium were collected, centrifuge-clarified and stored in aliquots at -80°C. lentiviral transduction of SH-SY5Y cells was performed in the presence of 4 µg/ml polybrene at MOI of 1.0. The medium was changed 24 h later, and the cells were cultured for an additional 48 h prior to further selection with 2 µg/ml puromycin for 3 days. Stable transfectants from a mixed population were used in the experiments.

Co-immunoprecipitation and Western Blot Analysis

Trypsinized SH-SY5Y cells were pelleted, washed with ice-cold phosphate-buffered saline (PBS), and then lysed in cell lysis buffer (Cell Signaling Technology, Cat #: 9803; 50 mM Tris-HCl, pH 7.5, 150 mM NaCl, 1 mM EDTA, 1 mM EGTA, 1% Nonidet P-40) containing 2.5 mM sodium pyrophosphate, 1 mM glycerophosphate, 1 mM Na_3VO_4, 1 µg/mL leupeptin, and additional protease Inhibitor cocktail (Sigma-Aldrich, P8340). Cell lysates were centrifuged at 16,000x g at 4°C for 10 min and protein concentration was determined using the BCA assay (Thermo Scientific).

For co-immunoprecipitation, the supernatants containing equal amounts of proteins were added to 1:1 Protein A and G Dyna beads (Thermo Fisher Scientific) mixture and incubated with anti-FLAG M2 antibody (Sigma Aldrich, F1804) by rotation overnight at 4°C. The bead-antibody-protein complex was washed thrice with lysis buffer. After the final washing, the beads were resuspended and boiled in Laemmli buffer before western blot analysis was performed.

For western blots, proteins were resolved on 4-20% Criterion TGX precast SDS-PAGE gels (Bio-Rad) and electro-transferred to polyvinylidene difluoride (PVDF) membranes (Millipore). The membranes were blocked for 1 h at room temperature with Odyssey blocking buffer (LI-COR) and incubated overnight at 4°C with primary antibodies. After incubation with IRDye 680/800-conjugated secondary antibodies, the membranes were scanned using an Odyssey infrared imaging system (LI-COR). The following primary antibodies were used: anti-SEPHS1 (Abcam, ab96542), anti-FLAG M2 (Sigma Aldrich, F1804) and anti-αTubulin (Genscript, A01622).

Cell Viability Assay

The alamar Blue viability assay was performed to assess the effect of *SEPHS1* mutants on cell viability. SH-SY5Y cells were seeded (1×10^4 cells/well) in Corning Costar 96-well, cell culture-treated, flat-bottom microplates (Day 0) and allowed to recover overnight at 37°C with 5% CO_2. For growth curve detection, 10 µL of alamarBlue HS cell viability reagent (Invitrogen, A50100) was added to the wells containing 100 µL of complete growth media and the attached cells. Cell plates were incubated at 37°C for exactly 2 hours prior to reading the fluorescence on days 1 - 7. Fluorescence was measured with excitation and emission values of 560 nm and 590 nm, respectively, using microplate reader Tecan infinite M200. Readings relative to Day 1 (100%) were used to plot against time.

Intracellular ROS Detection
Intracellular ROS levels were determined by using CellROX Deep Red Flow Cytometry Assay Kit (Thermo Scientific). Briefly, SH-SY5Y cells were treated with PBS or the common inducer of ROS production tert-butyl hydroperoxide (TBHP, 200 μM) for 30 minutes before labeling with the CellROX Deep Red reagent. The SYTOX Blue Dead Cell stain was further used to differentiate live cells from dead cells. Stained samples were analyzed by flow cytometry using Becton Dickinson LSRFortessa cytometer and FlowJo software (v10.9.0).

RNA Extraction and Quantitative Real-time PCR (qRT-PCR)
Total RNA was isolated using TRI reagent (Sigma-Aldrich, T9424). For gene expression analyses, 2.5 μg of RNA was reverse transcribed using iScript gDNA Synthesis Kit (Bio-Rad) in a 20 μl reaction mixture. The cDNA product was amplified using Sso Advanced SYBR Green Supermix (Bio-Rad) with gene-specific primers (Table S2). The PCR plates were denatured for 3 min at 95 °C and then subjected to 40 cycles of 10 s at 95 °C and 30 s at 60 °C in a CFX96 real-time PCR detection system (Bio-Rad). PCR products were subjected to melting curve analysis to assure that a single amplification product was produced. Quantification of relative changes in mRNA level was determined by the ΔΔCt method (normalized to DNA polymerase beta, POLB) and expressed as the fold change between experimental and control samples.

Statistical Analysis
Data analysis was performed in GraphPad Prism version 9.5.1 (GraphPad Software, San Diego, California USA, www.graphpad.com). For multiple group experiments, ANOVA was used with Dunnett's multiple comparisons test for group-wise comparison. P values > 0.05 were not statistically significant (ns).

References:

1. Retterer, K., Juusola, J., Cho, M.T., Vitazka, P., Millan, F., Gibellini, F., Vertino-Bell, A., Smaoui, N., Neidich, J., Monaghan, K.G., et al. (2016). Clinical application of whole-exome sequencing across clinical indications. Genet Med *18*, 696-704. 10.1038/gim.2015.148.
2. Soden, S.E., Saunders, C.J., Willig, L.K., Farrow, E.G., Smith, L.D., Petrikin, J.E., LePichon, J.B., Miller, N.A., Thiffault, I., Dinwiddie, D.L., et al. (2014). Effectiveness of exome and genome sequencing guided by acuity of illness for diagnosis of neurodevelopmental disorders. Sci Transl Med *6*, 265ra168. 10.1126/scitranslmed.3010076.
3. Kernohan, K.D., Hartley, T., Naumenko, S., Armour, C.M., Graham, G.E., Nikkel, S.M., Lines, M., Geraghty, M.T., Richer, J., Mears, W., et al. (2018). Diagnostic clarity of exome sequencing following negative comprehensive panel testing in the neonatal intensive care unit. Am J Med Genet A *176*, 1688-1691. 10.1002/ajmg.a.38838.
4. Yang, J., Tian, B., Sun, H., Garofalo, R.P., and Brasier, A.R. (2017). Epigenetic silencing of IRF1 dysregulates type III interferon responses to respiratory virus infection in epithelial to mesenchymal transition. Nat Microbiol *2*, 17086. 10.1038/nmicrobiol.2017.86.